Check for updates

GP73 is a glucogenic hormone contributing to SARS-CoV-2-induced hyperglycemia

Luming Wan [1,8], Qi Gao [2,8], Yongqiang Deng [3,8], Yuehua Ke [4,8], Enhao Ma [5,8], Huan Yang [1,6,8], Haotian Lin [1,8], Huilong Li [1,6], Yilong Yang [1], Jing Gong [1], Jingfei Li [1], Yixin Xu [1], Jing Liu [1], Jianmin Li [1], Jialong Liu [1], Xuemiao Zhang [1], Linfei Huang [1], Jiangyue Feng [1], Yanhong Zhang [1], Hanqing Huang [1], Huapeng Wang [1], Changjun Wang [4], Qi Chen [3], Xingyao Huang [3], Qing Ye [3], Dongyu Li [1], Qiulin Yan [1], Muyi Liu [1], Meng Wei [1], Yunhai Mo [1], Dongrui Li [1], Ke Tang [1], Changqing Lin [2], Fei Zheng [2], Lei Xu [2], Gong Cheng [5], Peihui Wang [7], Xiaopan Yang [1,9], Feixang Wu [6,9], Zhiwei Sun [2,9], Chengfeng Qin [3,9], Congwen Wei [1,9] and Hui Zhong [1,9] ✉

Severe cases of infection with severe acute respiratory syndrome coronavirus 2 (SARS-CoV-2) are associated with elevated blood glucose levels and metabolic complications. However, the molecular mechanisms for how SARS-CoV-2 infection alters glycometabolic control are incompletely understood. Here, we connect the circulating protein GP73 with enhanced hepatic gluconeogenesis during SARS-CoV-2 infection. We first demonstrate that GP73 secretion is induced in multiple tissues upon fasting and that GP73 stimulates hepatic gluconeogenesis through the cAMP/PKA signaling pathway. We further show that GP73 secretion is increased in cultured cells infected with SARS-CoV-2, after overexpression of SARS-CoV-2 nucleocapsid and spike proteins and in lungs and livers of mice infected with a mouse-adapted SARS-CoV-2 strain. GP73 blockade with an antibody inhibits excessive glucogenesis stimulated by SARS-CoV-2 in vitro and lowers elevated fasting blood glucose levels in infected mice. In patients with COVID-19, plasma GP73 levels are elevated and positively correlate with blood glucose levels. Our data suggest that GP73 is a glucogenic hormone that likely contributes to SARS-CoV-2-induced abnormalities in systemic glucose metabolism.

Under physiological conditions, blood glucose levels are maintained within a narrow range to prevent hypoglycemia during fasting and excessive hyperglycemia following intake of a high-carbohydrate meal[1]. Glucose homeostasis is achieved primarily via hormonal modulation of glucose production by the liver[2] and glucose uptake by skeletal muscle, heart muscle and adipose tissue[3,4]. Hepatic glucose production (HGP) involves a combination of glycogen breakdown (glycogenolysis) and de novo synthesis of glucose from noncarbohydrate precursors (gluconeogenesis)[2]. Gluconeogenesis is the main contributor to hepatic and renal glucose production during prolonged fasting states[5]. The rate of gluconeogenic flux is controlled by the activities of key unidirectional enzymes, such as pyruvate carboxylase (PCX), phosphoenolpyruvate carboxykinase 1 (PCK1), fructose 1,6-bisphosphatase (FBP1) and glucose-6-phosphatase (G6Pase)[6]. The genes encoding these proteins are strongly controlled at the transcriptional level by key hormones, including insulin, glucagon and glucocorticoids[7]. Excessive HGP not only contributes to exaggerated fasting and postprandial hyperglycemia in patients with type 1 diabetes (T1D) and type 2 diabetes (T2D) but also contributes to stress-, infection- and inflammation-associated hyperglycemia[8,9].

Since January 2020, the world has been facing an unprecedented outbreak of coronavirus disease 2019 (COVID-19) caused by SARS-CoV-2. Recent clinical data have suggested a close interaction between COVID-19 and diabetes[10–14]. Preexisting diabetes substantially increases COVID-19 mortality and morbidity. An increase in new-onset hyperglycemia, diabetic ketoacidosis (DKA) and diabetes in patients with COVID-19 is commonly observed. Although impaired insulin secretion due to β-cell infection could plausibly contribute to the metabolic dysregulation observed in patients with COVID-19 (refs. [15–17]), the pathogenic mechanisms underlying new-onset T2D are largely unknown.

GP73 is a type II transmembrane Golgi protein located at the luminal surface of the Golgi apparatus, consisting of a short N-terminal cytoplasmic domain, a transmembrane domain and a large C-terminal domain[18]. GP73 cycles out of the *cis*-Golgi to endosomes for cleavage by the convertase furin, resulting in its release into the extracellular space[19,20]. Circulating GP73 is implicated in the regulation of cell-to-cell communication triggered by the unfolded protein response[21]. The present study provides evidence that circulating GP73 promotes HGP in endocrine and autocrine manners. Notably, plasma GP73 levels are elevated in patients with

[1]Beijing Institute of Biotechnology, Academy of Military Medical Sciences (AMMS), Beijing, China. [2]Beijing Sungen Biomedical Technology Co. Ltd., Beijing, China. [3]Beijing Institute of Microbiology and Epidemiology, AMMS, Beijing, China. [4]Centers for Disease Control and Prevention of PLA, Beijing, China. [5]Tsinghua-Peking Center for Life Sciences, School of Medicine, Tsinghua University, Beijing, China. [6]Department of Hepatobiliary Surgery, Affiliated Tumor Hospital of Guangxi Medical University, Nanning, China. [7]Key Laboratory for Experimental Teratology of Ministry of Education and Advanced Medical Research Institute, Cheeloo College of Medicine, Shandong University, Jinan, China. [8]These authors contributed equally: Luming Wan, Qi Gao, Yongqiang Deng, Yuehua Ke, Enhao Ma, Huan Yang, Haotian Lin. [9]These authors jointly supervised this work: Xiaopan Yang, Feixang Wu, Zhiwei Sun, Chengfeng Qin, Congwen Wei, Hui Zhong. ✉e-mail: towall@yahoo.com
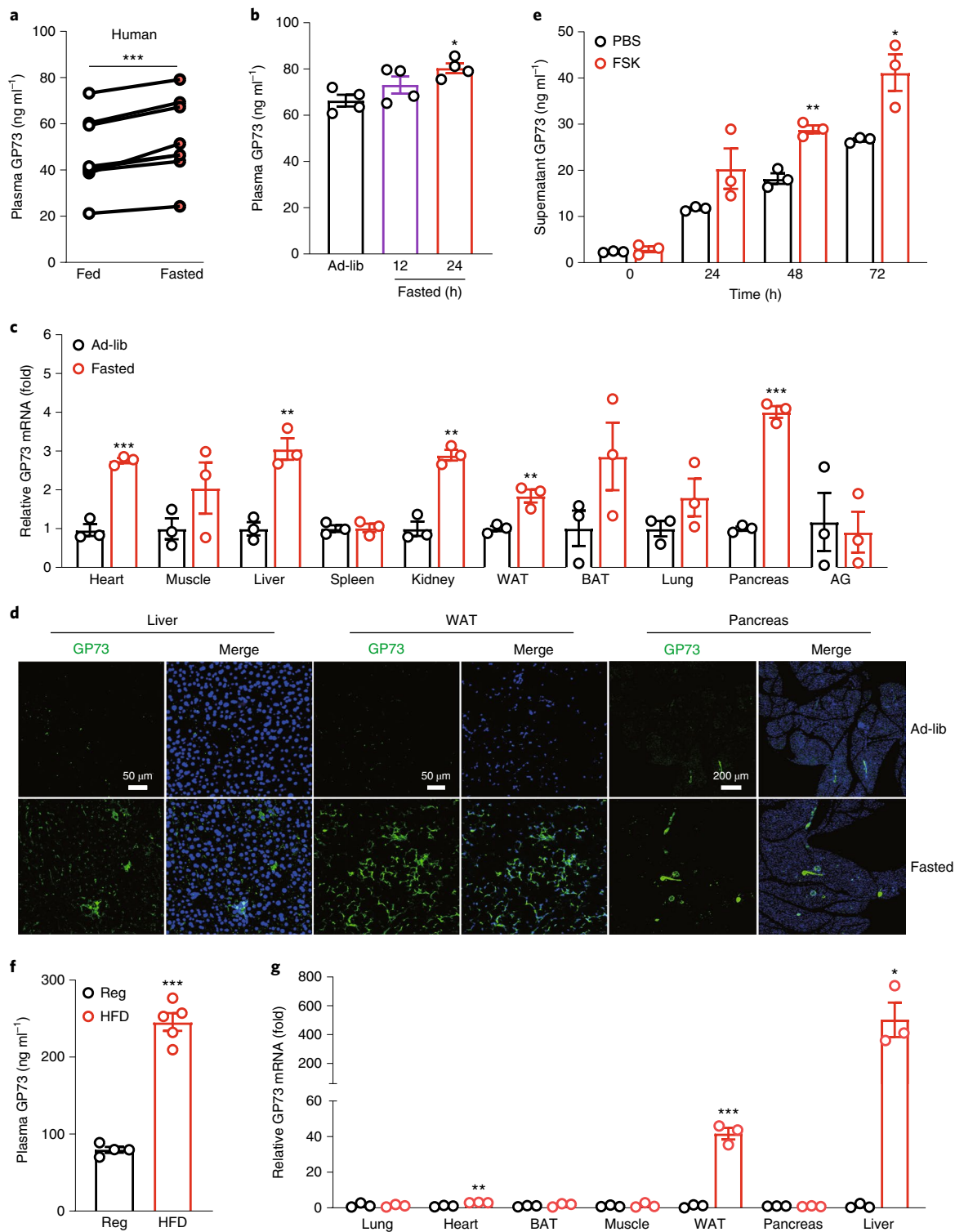
Fig. 1 | GP73 is induced from multiple tissues upon fasting and HFD. a,b, Plasma GP73 levels in humans following an overnight fast (**a**; $n = 7$) or in mice fed ad libitum (ad-lib) or fasted for the indicated times (**b**; $n = 4$). $P = 0.0005$ for fasted versus fed by two-tailed paired Student's t-tests (**a**), $P = 0.0180$ for fasted (24 h) versus ad-lib by one-way analysis of variance (ANOVA) followed by Bonferroni's post hoc test (**b**). **c**, GP73 mRNA expression in various organs from mice fed ad-lib or fasted for 24 h. BAT, brown adipose tissue; AG, adrenal gland ($n = 3$). $P = 0.0004$ for fasted heart versus ad-lib, $P = 0.0031$ for fasted liver versus ad-lib, $P = 0.0012$ for fasted kidney versus ad-lib, $P = 0.0097$ for fasted WAT versus ad-lib, $P < 0.0001$ for fasted pancreas versus ad-lib by two-tailed Student's t-tests. **d**, Representative of three confocal immunofluorescence images of GP73 staining in liver, WAT and pancreatic sections from three mice fed ad libitum or fasted for 24 h. Green represents GP73 and blue represents the nucleus. **e**, Supernatant GP73 levels in HepG2 cells treated with FSK (20 μM) for the indicated times. $P = 0.0018$ for FSK versus PBS (48 h), $P = 0.0218$ for FSK versus PBS (72 h) by two-tailed Student's t-tests. **f,g**, Plasma GP73 levels (**f**) or GP73 mRNA expression in various organs in mice fed a regular diet (reg) or HFD for 4 months (**f**, $n = 4$ or 5 in each group; **g**, $n = 3$). $P < 0.0001$ for HFD versus reg (**f**) by two-tailed Student's t-tests. $P = 0.0010$ for fasted heart versus ad-lib, $P = 0.0002$ for fasted WAT versus ad-lib, $P = 0.0135$ for fasted liver versus ad-lib by two-tailed Student's t-tests (**g**). Animal and cell-based studies were performed independently at least three biological replicates with comparable results. Data are mean ± s.e.m. *$P < 0.05$, **$P < 0.01$, ***$P < 0.001$.

COVID-19 and GP73 is necessary for excessive glucogenesis stimulated by SARS-CoV-2 infection. Therefore, targeting GP73 might be a potential therapeutic strategy for patients presenting alterations in the levels of this hormone.

Results

GP73 is induced from multiple tissues upon fasting and high-fat diet. A previous report showed that GP73 is cleaved at the R[52]VRR[55] proprotein convertase (PC) consensus site by the protease furin, resulting in its release into the extracellular space[19,20]. The elevated serum GP73 levels in patients with nonalcoholic steatohepatitis (NASH) prompted us to examine the potential metabolic function of circulating GP73 (ref. [22]). We first monitored to investigate whether circulating GP73 levels change in response to nutrient fluctuations. Indeed, fasting in humans and mice increased plasma GP73 levels (Fig. 1a,b). As intracellular GP73 overexpression led to the release of GP73 into the extracellular space (Extended Data Fig. 1a,b), we examined and compared GP73 expression in metabolically important organs isolated from ad libitum-fed and fasted mice to delineate the source of GP73 under fasting conditions. After 24 h of fasting, a strong upregulation of GP73 messenger RNA expression in the heart, liver, kidney, white adipose tissue (WAT) and pancreas was observed (Fig. 1c). Consistent with this finding, the intensity of GP73 immunofluorescence staining in liver, WAT and pancreatic tissues was significantly increased upon 24 h of fasting (Fig. 1d). GP73 secretion from cultured HepG2 cells was also promoted in response to the fasting-related signal forskolin (FSK; Fig. 1e). Fasting-related secretion of GP73 prompted us to examine circulating GP73 levels in the context of metabolic disturbance. Notably, plasma GP73 was markedly increased (approximately threefold) in mice fed a high-fat diet (HFD; Fig. 1f). In particular, HFDs induced dramatically increased GP73 mRNA expression in heart, liver and WAT tissues (Fig. 1g). Thus, GP73 secretion is induced from multiple tissues upon nutrient fluctuations.

Increase in circulating GP73 elevates fasting blood glucose. To understand the acute response to elevated circulating GP73 levels, we expressed and purified the mouse GP73 C-terminal fragment (56–401; rmGP73) (Extended Data Fig. 2a,b). A mouse GP73 sandwich ELISA was developed and specificity was confirmed using plasma from wild-type (WT) and GP73 knockout (KO) mice (Extended Data Fig. 2c,d). Administration of a single dose of 0.1 mg kg⁻¹ rmGP73 led to an approximately twofold increase in plasma GP73 levels compared to control mice, with a half-life of approximately 30 min (Extended Data Fig. 2e,f). We then experimentally elevated plasma GP73 levels via intravenous (i.v.) injection of 0.1 mg kg⁻¹ rmGP73 into mice subjected to a preceding 12-h

fast. In this setting, rmGP73 induced an immediate spike in blood glucose levels and compensatory hyperinsulinemia (Fig. 2a,b). A GP73-specific antibody completely blocked the glucose-stimulating effect of recombinant GP73 (Fig. 2c). Interestingly, GP73 treatment had no effect on plasma levels of glucagon, catecholamines and glucocorticoids, catabolic hormones known to induce hepatic glucose release (Extended Data Fig. 3a–d). We then injected rmGP73 daily for 3 d. Repeated GP73 injection produced a sharp rise in blood glucose levels (Fig. 2d).

Hyperglycemia is caused either by impaired glucose clearance and/or excess glucose production through glycogenolysis or gluconeogenesis. To determine which of these processes caused GP73-induced hyperglycemia, we performed an insulin tolerance test (ITT). There were no significant differences in mice challenged with rmGP73 (Fig. 2e). However, when we assessed insulin resistance with the glucose tolerance test (GTT), we observed that rmGP73 severely impaired glucose clearance (Fig. 2f). The pyruvate tolerance test (PTT) indicated that the conversion of pyruvate to glucose was greatly enhanced after GP73 challenge in overnight-fasted, glycogen-depleted mice and that this effect was completely blocked by anti-GP73 treatment (Fig. 2g). GP73 elevation also stimulated alanine-driven gluconeogenesis in a glycogen-depleted state (Fig. 2h). No significant difference was found in hepatic glycogen content between the rmGP73- and GFP-injected mice (Extended Data Fig. 3e), suggesting that glycogenolysis was not affected by GP73. In particular, neutralizing circulating GP73 with a GP73 mAb in fasting animals attenuated the ability of mice to maintain normoglycemia (Fig. 2i). Notably, GP73 treatment tended to decrease insulin-stimulated phosphorylation of AKT at Ser473 in primary mouse hepatocytes (PMHs), HepG2 cells and L6 rat myotubes (Fig. 2j). Thus, an increase in circulating GP73 may elevate fasting glycemia mainly by potentiating endogenous glucose production and reducing glucose clearance (Extended Data Fig. 3f).

Circulating GP73 traffics to the liver to stimulate gluconeogenesis. To examine the primary target of circulating GP73, rmGP73 labeled with Cy7 (rmGP73-Cy7) was injected into mice and an in vitro imaging system (IVIS) was used to identify sites of accumulation. In contrast to free Cy7, rmGP73-Cy7 trafficked primarily to the liver and kidney (Extended Data Fig. 4a) and exhibited higher accumulation in these two tissues 30 min after injection (Fig. 3a and Extended Data Fig. 4b). In addition, the fluorescence signal in the liver 19 h after administration was 20% of the signal at 1 h (Extended Data Fig. 4c,d). Moreover, GP73 bound to the surface of hepatocytes in a dose-dependent and saturable manner (Fig. 3b and Extended Data Fig. 4e).

Fig. 2 | Increase in circulating GP73 elevates fasting blood glucose. a, Plasma glucose levels at the indicated times after a single dose of i.v. rmGP73 (0.1 mg kg⁻¹) or PBS in mice subjected to a preceding 12 h fast (n = 6). P = 0.0047 for rmGP73 versus PBS (15 min), P = 0.0065 for rmGP73 versus PBS (30 min), P < 0.0001 for rmGP73 versus PBS (60 min), P = 0.0084 for rmGP73 versus PBS (90 min) and P = 0.0018 for rmGP73 versus PBS (120 min) by two-way ANOVA followed by Bonferroni's post hoc test. **b,** Plasma insulin levels 15 min after rmGP73 injection (n = 6). P < 0.0001 for rmGP73 versus PBS (15 min) by two-tailed Student's t-tests. **c,** Plasma glucose levels 15 min after rmGP73 injection with IgG isotype or anti-GP73 antibody (n = 5). P = 0.0027 for rmGP73 versus PBS (isotype), P = 0.0067 for anti-GP73 versus isotype (rmGP73) by one-way ANOVA followed by Bonferroni's post hoc test. **d,** Plasma glucose levels at the indicated times after rmGP73 injection once daily for 3 d (n = 6). P = 0.0016 for first versus PBS, P < 0.0001 for second versus PBS, P = 0.0020 for third versus PBS by two-way ANOVA followed by Bonferroni's post hoc test. **e–h,** ITT (**e**), intravenous glucose tolerance test (IGTT; **f**), PTT with or without anti-GP73 antibody (**g**) or alanine tolerance test (ATT; **h**) in mice 2 h after rmGP73 injection (n = 5 or 6). P = 0.6384 for rmGP73 versus PBS by two-way ANOVA test (**e**), P < 0.0001 for rmGP73 versus PBS (30 min and 60 min), P = 0.0012 for rmGP73 versus PBS (90 min), P = 0.0176 for rmGP73 versus PBS (120 min) by two-way ANOVA followed by Bonferroni's post hoc test (**f**), P < 0.0001 for rmGP73 + anti-GP73 versus rmGP73 + isotype (15 min, 30 min, 60 min, 90 min and 120 min) (**g**), P = 0.0046 for rmGP73 versus PBS (0 min), P = 0.0126 for rmGP73 versus PBS (15 min), P = 0.0063 for rmGP73 versus PBS (30 min) (**h**) by two-way ANOVA followed by Bonferroni's post hoc test. **i,** Plasma glucose levels 15 min after injection of IgG isotype or anti-GP73 antibody in mice subjected to a preceding 12 h fast (n = 5). P = 0.0036 for anti-GP73 versus isotype by two-tailed Student's t-tests. **j,** Immunoblotting (IB) analysis of AKT phosphorylation (AKT-p) in PMHs, HepG2 or L6 cells treated with the indicated concentrations of insulin in the presence or absence of GP73. Animal and cell-based studies were performed independently at least three biological replicates with comparable results. Data are mean ± s.e.m. *P < 0.05, **P < 0.01, ***P < 0.001.

We then directly assessed the effect of GP73 on glucose production in isolated PMHs. Treatment of PMHs isolated from overnight-fasted mice with rmGP73 promoted HGP in a dose- and time-dependent manner (Fig. 3c and Extended Data Fig. 5a). A similar result was observed in rat primary hepatocytes treated with recombinant rat GP73 (rrGP73; Extended Data Fig. 5b). In particular, a GP73-specific antibody blocked GP73-mediated hepatocyte glucose release (Extended Data Fig. 5c). Small molecular inhibitors of PKA, such as cAMPS-Rp and H89, completely blocked GP73-mediated hepatocyte glucose release in a similar manner as glucagon (Fig. 3d). In addition, we found that insulin exerted some suppressive effect on GP73-mediated glucose release (Fig. 3d). While the glucagon receptor (GCGR) allosteric antagonist LY2409021 completely blocked the effects of glucagon, it also partially suppressed the ability of GP73 to stimulate hepatocyte glucose release (Fig. 3d). The addition of rmGP73 also led to increased expression of key gluconeogenic enzymes, intracellular cAMP levels and PKA kinase activity (Fig. 3e and Extended Data Fig. 5d,e). Phosphorylation of the PKA-C-α subunit and PKA substrate levels in hepatocytes was also significantly increased by GP73 (Fig. 3f). Notably, rmGP73 addition in primary hepatocytes isolated from overnight-fasted GP73 KO mice was sufficient to completely rescue the HGP deficiency displayed by these cells (Fig. 3g).
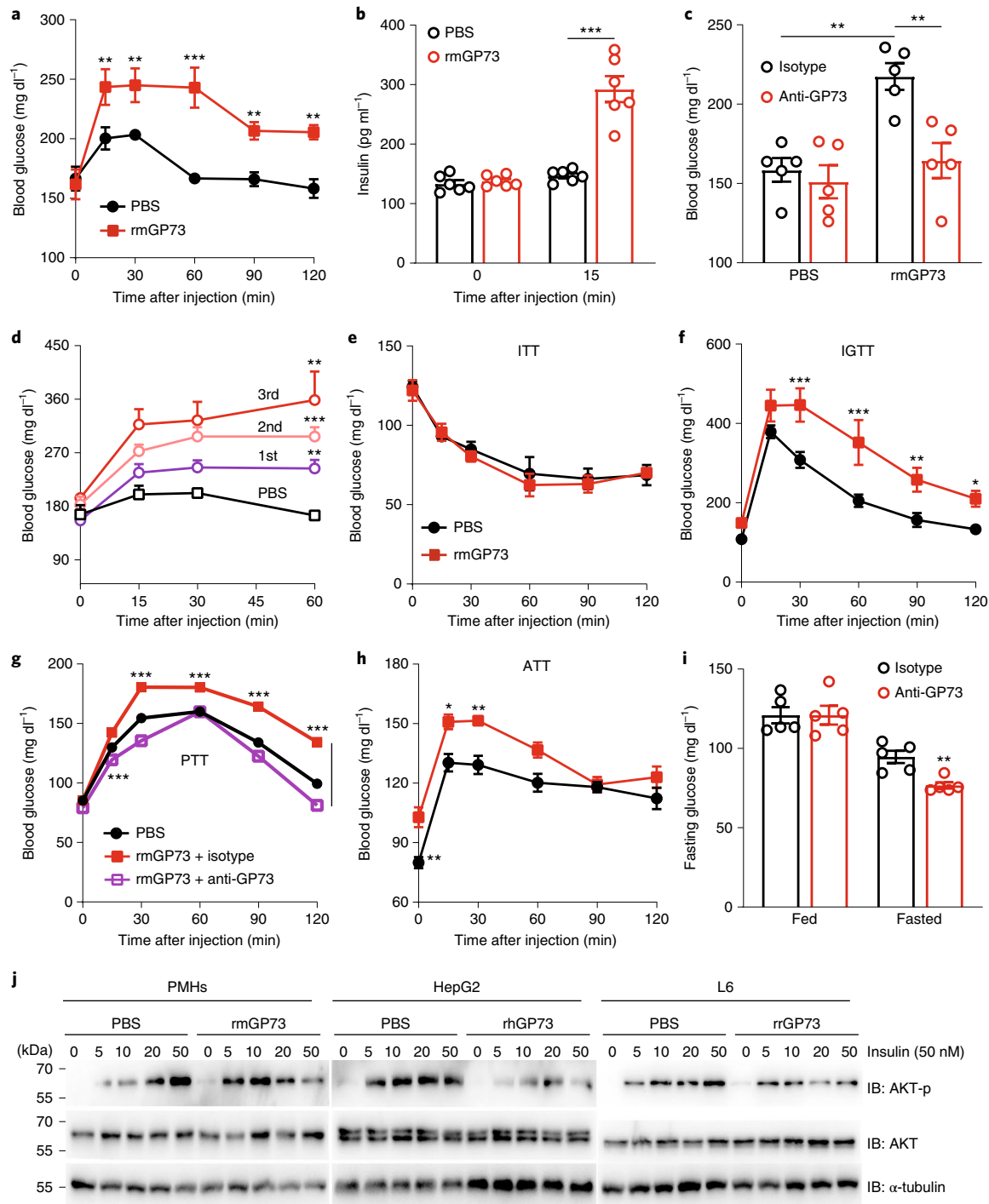
We next performed hyperinsulinemic-euglycemic clamp studies in GP73-deficient genetic background mice (GP73 KO) and reconstituted circulating GP73 by infusing recombinant protein (Fig. 3h–j and Extended Data Fig. 6a–f). We were able to achieve blood GP73 levels comparable to those in WT animals (Extended Data Fig. 6c). In this setting, we found increased HGP and decreased whole-body glucose disposal (insulin sensitivity) upon GP73 administration (Fig. 3h,i).

GP73 induces a drastic remodeling of the PKA kinase hub. To determine the full extent of the hepatic signaling effect of circulating GP73 at the cellular level in the absence of systemic factors that may exert compensatory effects, we performed global phosphoproteomics analysis in PMHs treated with PBS, rmGP73 or glucagon in vitro. A total of 183 and 229 phosphosites were identified in the GP73-treated and glucagon-treated samples, respectively (Fig. 4a). Of the top 30 phosphosites that were highly upregulated by GP73, over 75% were also affected by glucagon (Fig. 4b), indicating that these two proteins have overlapping functions at the signaling level. Among the potentially functional phosphosites regulated by GP73, Ser1588 of inositol triphosphate receptor-1 (Itpr1, also known as InsP3R-I) attracted our attention (Fig. 4c). This protein is a target of PKA and plays a crucial role in glucagon-stimulated hepatic gluconeogenesis. Other proteins significantly regulated by GP73 that are known to be involved in gluconeogenesis signaling included PHKA2^{S729}, GNMT^{Y221}, SLC16A1^{S491}, MLX^{S45}, BAD^{S155}, CTNNB1^{S552}, GPX1^{S7}, CYP2E1^{S129} and HCFC1^{S1516} (Fig. 4c).

To investigate the mechanisms responsible for the phosphoproteome changes, kinase–substrate motifs were extracted and a clear shift toward PKA kinase activation following GP73 or glucagon stimulation was identified (Fig. 4d and Extended Data Fig. 7a). Pathway analysis of the phosphosites regulated by GP73 revealed pathways related to cell–cell adhesion, cell endocytosis, mRNA processing, gene transcription and cell cycle regulation (Extended Data Fig. 7b). Other substrate motifs of key kinases previously implicated in the regulation of gluconeogenesis and insulin resistance, including GSK3B, PRKG1, PTK2B and CaMK2A, were also dysregulated, which further explains the ability of GP73 to affect glucose production and insulin sensitivity (Fig. 4e). Additional enriched kinase motifs following GP73 stimulation included mitogen-activated kinase (MAPK) 3/8/9/10/13/14 and cyclin-dependent kinase (CDK)1/2 (Fig. 4e). Global kinase enrichment analysis following GP73 stimulation revealed that GP73 induced drastic remodeling of the PKA hub in a similar manner as glucagon (Extended Data Fig. 8a,b). At the signaling level, the mTOR pathway, FoxO pathway and insulin pathway were positively enriched in GP73-treated

hepatocytes (Fig. 4f). Therefore, GP73 induces drastic remodeling of the PKA kinase hub and multiple signaling pathways.

SARS-CoV-2 infection promotes GP73 production and secretion. A proteomics analysis of patients with COVID-19 shows elevated expression of GP73 in the lung, liver and renal tissues[23], indicating a possible link between SARS-CoV-2 infection and GP73 expression. To assess whether infection with this virus altered GP73 secretion, Huh-7 cells were infected with SARS-CoV-2 (Extended Data Fig. 9a–c) and GP73 secretion was examined over time during infection. Cultured hepatocytes exposed to SARS-CoV-2 exhibited a robust dose- and time-dependent increase in GP73 secretion (Fig. 5a,b). Intracellular GP73 protein expression was also increased in SARS-CoV-2-infected cells (Fig. 5c). To further evaluate this finding in a mouse model infected with a mouse-adapted strain at passage 6 (ref. [24]) (MASCp6; Extended Data Fig. 9d), we examined and compared GP73 expression in multiple tissues from MASCp6- or mock-infected mice. On day 2 after infection, upregulation of GP73 expression in the lung and liver tissues was observed (Fig. 5d-e). Of note, the increased staining of GP73 occurred in lung cells stained positive with S-protein as well as in S-protein-negative neighboring cells, indicating that SARS-CoV-2 induced GP73 expression likely in both a direct and a paracrine manner (Extended Data Fig. 9e).

We then evaluated the effect of individual SARS-CoV-2 proteins on GP73 secretion. By screening 23 viral proteins, we found that the expression of the N and S proteins significantly promoted GP73 secretion, whereas the NSP12 and NSP14 proteins exhibited the opposite effects (Fig. 5f and Extended Data Fig. 9f). Notably, GP73 secretion was enhanced by the N protein in a dose-dependent manner (Fig. 5g and Extended Data Fig. 9g). HIV pseudotypes bearing SARS-2-S (SARS-CoV-2pp) also enhanced GP73 secretion when presented during infection compared to VSV-Gpp (Fig. 5h). Similar results were obtained in a panel of human cell lines (Extended Data Fig. 9h). Notably, both the N and S proteins coimmunoprecipitated with endogenous GP73 (Fig. 5i,j). Together, these results demonstrate that SARS-CoV-2 proteins regulate the secretion of GP73.

Plasma GP73 is pathologically elevated in patients with SARS-CoV-2 infection. We then examined plasma GP73 expression in patients with COVID-19. Notably, SARS-CoV-2-infected patients had approximately twofold higher circulating GP73 levels than the reference population (Supplementary Table 1 and Fig. 6a). When disease status was classified into mild, moderate and severe, the serum GP73 concentration was significantly higher in patients with severe or moderate disease than in patients with moderate

Fig. 3 | Circulating GP73 traffics to the liver to stimulate gluconeogenesis. a, In vivo imaging of various organs from two mice 30 min after rmGP73-Cy7 or free Cy7 injection. Two representative images from four mice are shown. **b**, The level of biotin on the hepatocyte surface upon incubation of HepG2 cells with increasing concentrations of rhGP73-biotin. Specific binding (shown in red) was calculated as the difference between the two curves. **c**, Glucose production in PMHs treated with rmGP73 at the indicated concentrations for 2 h. $P < 0.0001$ for 4 nM versus 0 nM, 8 nM versus 0 nM, 16 nM versus 0 nM, 32 nM versus 0 nM and 64 nM versus 0 nM by one-way ANOVA followed by Bonferroni's post hoc test. **d**, Glucose production in PMHs treated with 32 nM rmGP73 or glucagon in the presence of cAMPS-Rp (20 μM), H89 (20 μM), LY2409021 (2.5 μM), or insulin (10 μM) for 2 h. $P = 0.0070$ for rmGP73 + insulin versus rmGP73, $P = 0.0062$ for rmGP73 + LY2409021 versus rmGP73, $P = 0.0004$ for glucagon + insulin versus glucagon, $P < 0.0001$ for rmGP73 + H89 versus rmGP73, rmGP73 + cAMPS-Rp versus rmGP73, glucagon + insulin versus glucagon, glucagon + LY2409021 versus glucagon, glucagon + H89 versus glucagon and glucagon + cAMPS-Rp versus glucagon by one-way ANOVA followed by Bonferroni's post hoc test. **e**, Gluconeogenesis gene expression in PMHs treated with 32 nM rmGP73 for 2 h. $P = 0.0051$ for rmGP73 versus PBS (*Pcx*), $P < 0.0001$ for rmGP73 versus PBS (*Pck1* and *G6pc*) by two-tailed Student's *t*-tests. **f**, Immunoblotting analysis of phosphorylated PKA-C subunit (PKA-C-α-p) levels and substrate (phosphoRRXT*T*-PKA substrate, RRXpS/T) levels in HepG2 cells treated with 32 nM rmGP73 or 10 μM IBMX for the indicated times. DMSO, dimethylsulfoxide. **g**, Glucose production in PMHs isolated from WT or KO mice treated with or without rmGP73 (32 nM) for 4 h. $P = 0.0090$ for KO versus WT, $P < 0.0001$ for KO + rmGP73 versus KO by one-way ANOVA followed by Bonferroni's post hoc test. **h–j**, Basal and clamp HGP (**h**), glucose disposal rate (GDR) (**i**) and insulin levels (**j**) in GP73 KO mice infused with GFP or recombinant GP73 during the clamp study. $P = 0.0194$ for rmGP73 versus GFP (basal), $P = 0.0026$ for rmGP73 versus GFP (clamp) (**h**), $P = 0.0047$ for rmGP73 versus GFP (**i**) and $P = 0.8818$ for rmGP73 versus GFP (**j**) by two-tailed Student's *t*-tests. Animal and cell-based studies were performed independently at least three biological replicates with comparable results. Data are mean ± s.e.m. NS, not significant; *$P < 0.05$; **$P < 0.01$; ***$P < 0.001$.

or mild disease (Supplementary Table 2 and Fig. 6b). Indeed, blood glucose levels in patients with COVID-19 were higher than those in the reference population and were particularly higher in patients with severe disease (Fig. 6c,d). Notably, the plasma GP73 levels in patients with COVID-19 were positively correlated with blood glucose levels (Fig. 6e). It should be noted that the levels of GP73 and glucose levels remained elevated after recovery before discharge (Fig. 6f,g).

GP73 blockade inhibits SARS-CoV-2-induced gluconeogenesis enhancement. To assess whether pathologically elevated GP73 contributes to SARS-CoV-2-induced glucose abnormalities, we monitored the effect of SARS-CoV-2 on gluconeogenic activity. As expected, the induction of glucogenic gene expression and hepatocyte glucose production was significantly increased by SARS-CoV-2 infection (Fig. 7a,b). In contrast, the upregulated glucogenic gene expression and hepatocyte glucose production were all markedly
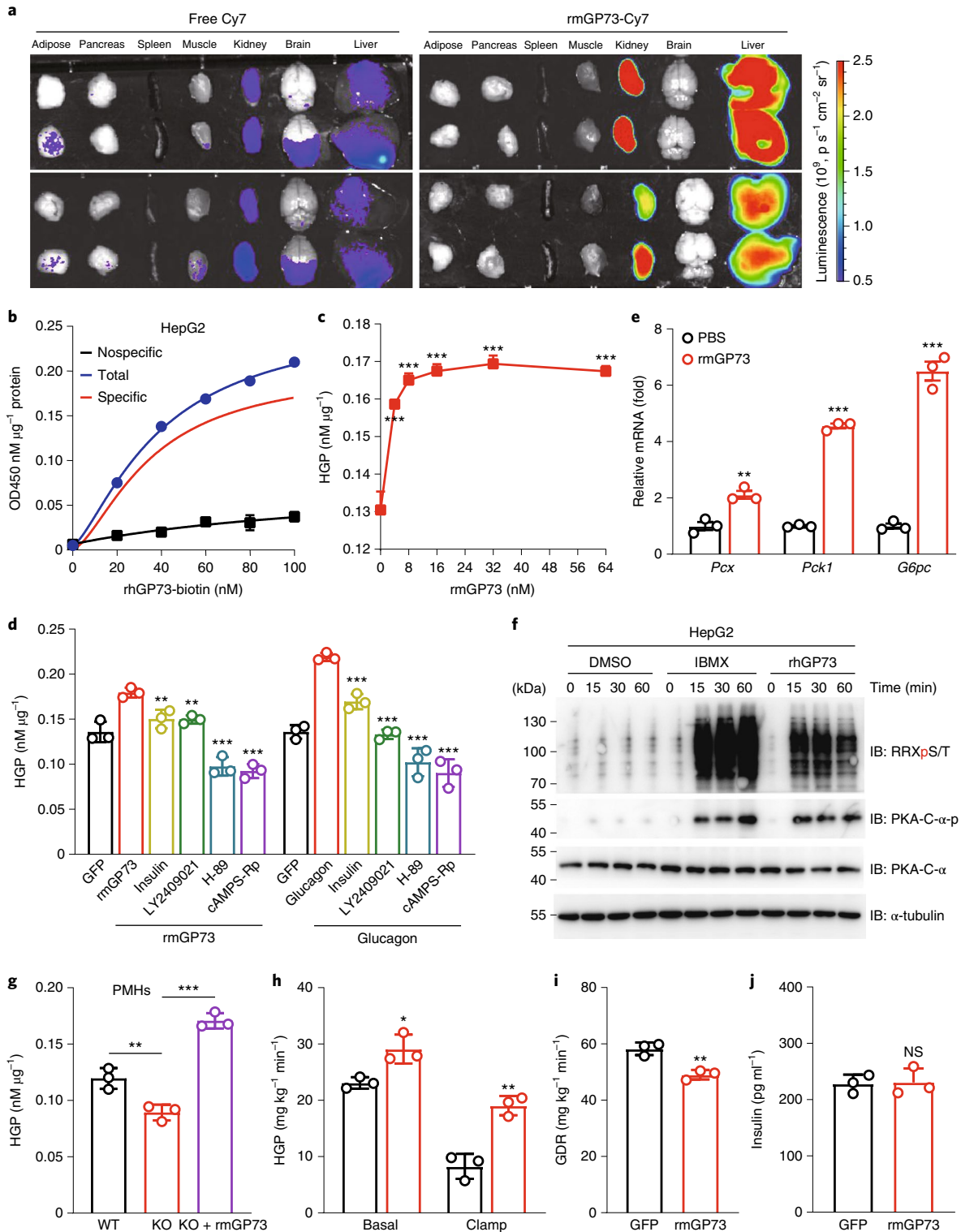
reduced by anti-GP73 antibody treatment (Fig. 7a,b), similar to the effect of GP73 depletion (Fig. 7c,d). Meanwhile, PKA activation by SARS-CoV-2 infection was also significantly blocked by a GP73-specific antibody (Fig. 6e). To further investigate whether the changes in serum GP73 were closely associated with gluconeogenesis levels, we obtained serum from patients with COVID-19

Fig. 4 | GP73 induces drastic remodeling of the PKA kinase hub. a, Overlapping numbers of significantly upregulated phosphopeptides and downregulated phosphopeptides in PMHs treated with rmGP73 (64 nM) or glucagon (3 μM) for 1 h. Localization probability ≥0.75 and fold-change ≥1.5 or fold-change ≤0.67 were declared significant. Significantly regulated phosphopeptides by GP73 are shown in blue and those regulated by glucagon are shown in red. **b**, Heat map of the top 30 highly upregulated phosphosites in PMHs treated with rmGP73. **c**, Network analysis of proteins involved in the glucogenesis signaling pathway in PMHs treated with rmGP73. Each of the phosphosites is color-coded based on fold change. Circular shapes show each protein that is upregulated in GP73-treated cells compared to PBS-treated cells. Lines indicate protein–protein interactions curated from databases of experimentally defined kinase–substrate relationships (STRING, confidence >0.7). **d,e**, Specific kinase–substrate motifs (**d**) or distribution of matching kinases (**e**) according to the phosphoproteomics data from the rmGP73-treated sample ($P < 0.05$) using MoMo (https://meme-suite.org/tools/momo) and Kinase Enrichment Analysis 2 (KEA2) based on one-tailed Fisher's exact test. **f**, KEGG enriched pathway analysis of significantly regulated phosphopeptides in PMHs treated with rmGP73 ($P < 0.05$) using DAVID Bioinformatics Resources 6.8. mTOR, Mammalian target of rapamycin; FoxO, Forkhead Box O; VEGF, Vascular endothelial growth factor; ErbB, Epidermal growth factor family of receptor tyrosine kinases; GnRH, Gonadotropin-releasing hormone. The bar plot shows significantly dysregulated pathways and one-tailed Fisher's exact test P values are shown on the x axis.

with GP73 levels higher than 60 ng ml^{-1} and age-matched healthy individuals with GP73 levels lower than 20 ng ml^{-1} and added the samples to culture medium. Glucogenic gene expression and PKA enzymatic activity were more strongly induced in cells exposed to serum from patients with COVID-19 than in cells exposed to serum from healthy controls and these effects were significantly blocked by anti-GP73 antibody (Fig. 7f,g).

We next demonstrated the relevance of these in vitro findings in a MASCp6-infected BALB/c mouse model. Compared with mock-infected control mice, MASCp6-infected mice exhibited elevated fasting blood glucose levels and increased hepatic G6pc expression on day 2 after inoculation (Fig. 7h,i). In contrast, pretreatment of MASCp6-infected mice with GP73-specific antibody led to a significant reduction in fasting blood glucose levels to approximately the same level as that seen in mock-infected mice (Fig. 7h). The upregulated G6pc expression in livers from MASCp6-infected mice was also markedly reduced by anti-GP73 antibody pretreatment (Fig. 7i). Thus, GP73 blockade inhibits SARS-CoV-2-induced increases in gluconeogenesis in vitro and lowers elevated fasting blood glucose levels in SARS-CoV-2-infected mice.

Discussion

The precise regulation of gluconeogenesis required for physiological adaptation to fasting and starvation and occurs at multiple levels[6,25]. In response to stimulation by external factors, circulating blood levels of insulin, glucagon and glucocorticoids change, leading to subsequent changes in glucogenic pathways and glucose production[26]. Here, we provide evidence linking circulating GP73 to hepatic gluconeogenesis. Consistent with the fact that hepatic glucose release is necessary during fasting, circulating concentrations of GP73 rise during fasting. Fasted mice in which GP73 is blockade fail to maintain normal blood glucose levels during the fasting period. Experimentally modulating the circulating GP73 concentration via direct recombinant protein injection or immunologic

sequestration results in corresponding changes in fasting plasma glucose. Mechanistically, secreted GP73 primarily targets the liver to promote gluconeogenesis via activation of PKA signaling in endocrine and autocrine manners. Notably, plasma GP73 levels are pathologically elevated in patients with COVID-19 and GP73 is essential for enhanced gluconeogenesis in response to SARS-CoV-2 infection. We thus proposed that the glucogenic property of GP73 might contribute to the hyperglycemia that occurs during SARS-COV-2 infection and in patients with COVID-19.

We assessed the direct actions of GP73 in the regulation of glucose production in primary hepatocytes in the absence of other counterregulatory hormones. GP73 was sufficient to cause cAMP accumulation, stimulate the enzymatic activity of PKA, increase the phosphorylation of CREB and enhance the transcriptional expression of *Pcx*, *Pck1* and *G6pc*. These results suggest that GP73 stimulates gluconeogenesis via the activation of PKA signaling through transcriptional regulation. In support of this hypothesis, we observed drastic remodeling of the PKA hub following GP73 challenge using phosphoproteomics. Likewise, phosphosites that were upregulated by glucagon were also significantly enriched with substrate motifs for PKA, indicating that glucagon and GP73 have overlapping functions at the signaling level. Among the potentially functional phosphosites regulated by GP73 and GCG, Itpr1 plays a crucial role in glucagon-stimulated hepatic gluconeogenesis, driving a metabolic program by stimulating intrahepatic lipolysis and increasing the mitochondrial fat oxidation process[27]. Therefore, GP73 may acutely stimulate gluconeogenesis by activating intrahepatic or WAT lipolysis in a transcription-independent alternative mechanism. Serving as a stimulator of HGP, a clamp study in vivo and insulin-induced AKT phosphorylation in vitro demonstrated a role of GP73 in regulating peripheral insulin sensitivity. The unaltered ITT indicates that GP73 might regulate insulin secretion in a context-dependent manner. Nevertheless, illustrating the potential role of GCGR as a receptor of GP73 to modulate HGP and

Fig. 5 | SARS-CoV-2 infection promotes GP73 production and secretion. a,b, Supernatant GP73 levels in Huh-7 cells infected with SARS-CoV-2 at the indicated multiplicity of infection (MOI) for 24 h (**a**) or with SARS-CoV-2 (MOI 0.1) for the indicated times (**b**). $P = 0.0177$ for 0.01 MOI versus 0 MOI, $P = 0.0002$ for 0.1 MOI versus 0 MOI (**a**), $P = 0.0049$ for 0.1 MOI versus 0 MOI (24 h), $P < 0.0001$ for 0.1 MOI versus 0 MOI (48 h), $P = 0.0010$ for 0.1 MOI versus 0 MOI (72 h) by two-way ANOVA followed by Bonferroni's post hoc test. **c**, Intracellular GP73 levels in Huh-7 cells infected with SARS-CoV-2 (CoV-2) at the indicated MOIs for 24 h. **d**, Representative of three confocal immunofluorescence images of GP73 staining in liver and lung sections from three MASCp6-infected mice. Green represents GP73 and blue represents the nucleus. **e**, GP73 mRNA expression in lung, liver and kidney tissues from mice inoculated with 1.6×10^4 plaque-forming units (p.f.u.) of MASCp6 and killed at day 2 after inoculation ($n = 6$). $P = 0.0079$ for infected versus mock (lung), $P = 0.0389$ for infected versus mock (liver) by two-tailed Student's t-tests. **f,g**, Supernatant GP73 levels in Huh-7 cells transfected with plasmids expressing the indicated SARS-CoV-2 proteins (**f**) or different concentrations of Flag-N (**g**). $P = 0.0097$ for NSP12 versus vector, $P = 0.0044$ for NSP14 versus vector, $P = 0.0012$ for S versus vector and $P = 0.0031$ for N versus vector by two-tailed Student's t-tests (**f**), $P = 0.0036$ for 0.5 μg versus 0 μg and $P < 0.0001$ for 4 μg versus 0 μg by one-way ANOVA followed by Bonferroni's post hoc test (**g**). **h**, Supernatant GP73 levels in Huh-7 cells challenged with SARS-CoV-2pp or VSV-Gpp for the indicated times. $P = 0.0205$ for SARS-2-Spp versus VSV-Gpp (12 h), $P = 0.0004$ for SARS-2-Spp versus VSV-Gpp (24 h) and $P = 0.0006$ for SARS-2-Spp versus VSV-Gpp (48 h) by two-way ANOVA followed by Bonferroni's post hoc test. **i,j**, Immunoprecipitation analysis of GP73 interaction with N (**i**) or S (**j**) protein in 293T cells transfected with Flag-N or Flag-S. Animal and cell-based studies were performed independently at least three biological replicates with comparable results. Data are mean ± s.e.m. *$P < 0.05$; **$P < 0.01$; ***$P < 0.001$.

identifying other potential cell-surface receptors through which GP73 exerts its effects may provide more mechanistic information.

Epidemiological and experimental data indicate that SARS-CoV-2 infection is associated with new-onset diabetes[28,29]. The mechanisms underlying this phenomenon are likely complex and may include the promotion of inflammation, structural lung damage and systemic effects[30]. The present study reported that SARS-CoV-2 infection was associated with insulin resistance via pathways involved in endogenous glucose production[31].

We demonstrated that enhanced gluconeogenic metabolism following SARS-CoV-2 infection was primarily dependent on GP73. In patients with COVID-19, as opposed to significantly elevated GP73 levels in patients with severe disease, serum GP73 levels in patients with mild disease were comparable to those observed in healthy controls, suggesting the presence of a threshold of disease severity or chronicity required for GP73 upregulation. Although the SARS-CoV-2 N and S proteins stimulated GP73 secretion, our data raise the question of whether GP73 expression is limited to
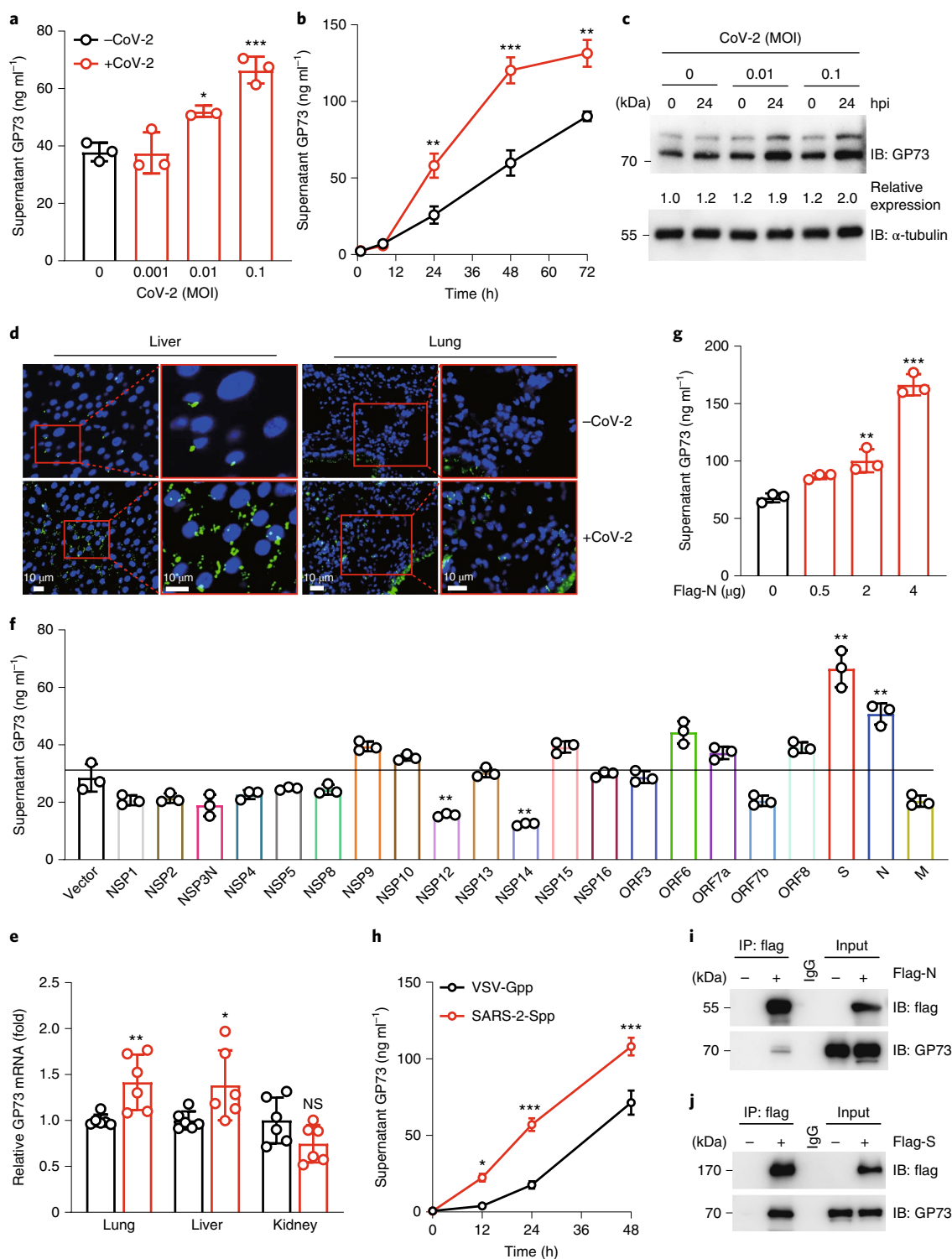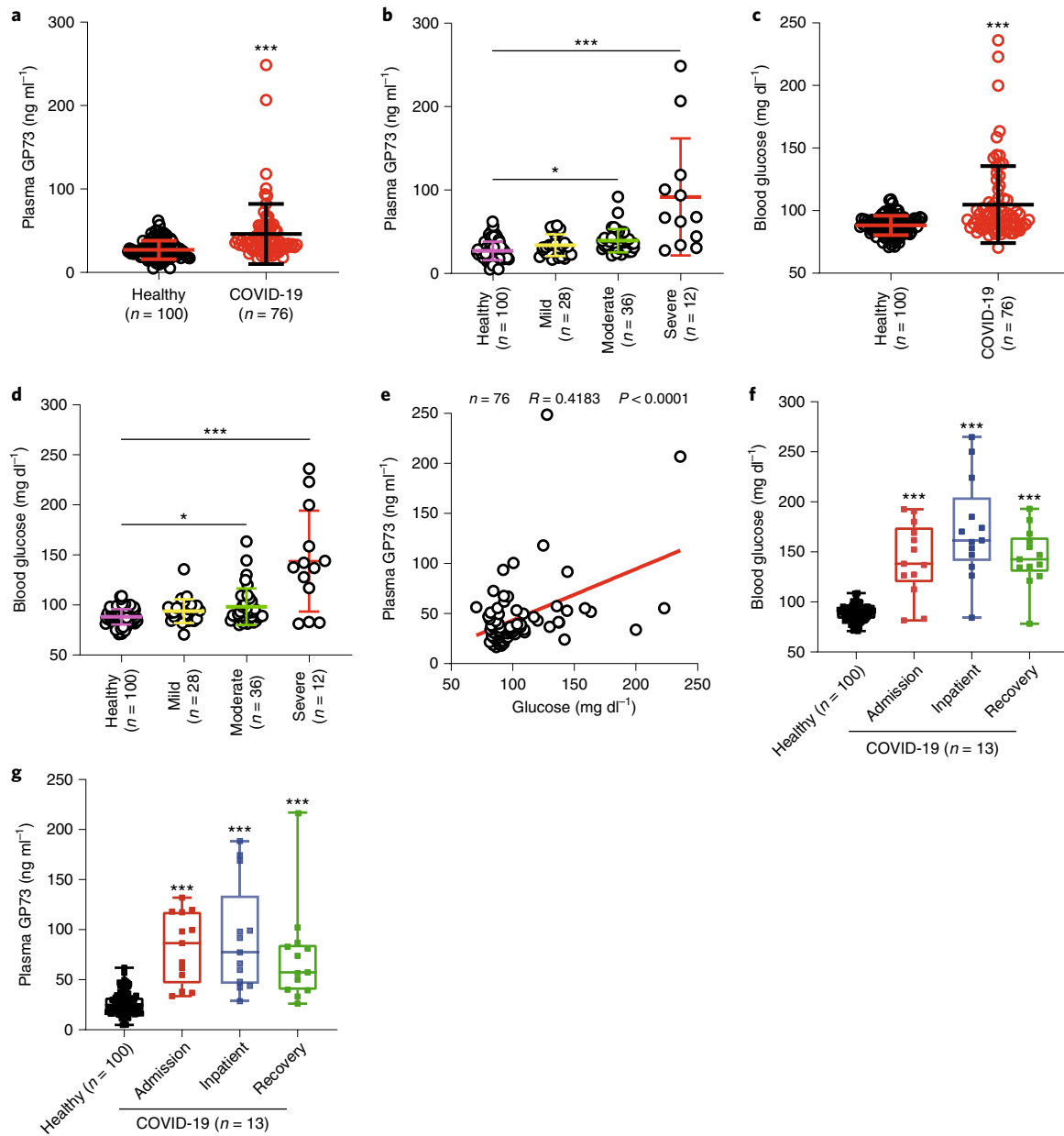
Fig. 6 | GP73 blockade inhibits SARS-CoV-2-induced gluconeogenesis enhancement. a–d, Plasma GP73 levels (**a**) or glucose levels (**c**) in healthy controls and patients with COVID-19. $P < 0.0001$ for COVID-19 versus healthy by two-tailed Student's t-tests (**a,c**). Plasma GP73 levels (**b**) or blood glucose levels (**d**) in healthy controls and patients with COVID-19 with different disease severities. $P = 0.0198$ for moderate versus healthy (**b**) and $P < 0.0001$ for severe versus healthy (**b**), $P = 0.0193$ for moderate versus healthy (**d**) and $P < 0.0001$ for severe versus healthy (**d**) by one-way ANOVA followed by Bonferroni's post hoc test. **e**, Correlation analysis between plasma GP73 levels and glucose levels in patients with COVID-19. $P < 0.0001$ by Pearson correlation analysis. **f,g**, Glucose levels (**f**) or plasma GP73 levels (**g**) in patients with COVID-19 at admission, inpatient and after recovery. In the box-and-whisker plots, the box represents the upper and lower quartiles and the line within the box is the mean. The whiskers represent the maximum and minimum values. $P < 0.0001$ for admission versus healthy, inpatient versus healthy and recovery versus healthy (**f,g**) by one-way ANOVA followed by Bonferroni's post hoc test. Data are mean ± s.e.m. *$P < 0.05$; ***$P < 0.001$.

SARS-CoV-2 replication. In fact, the levels of GP73 remained elevated after recovery. It has been observed that hyperglycemia persists for 3 years after recovery from SARS and can be detected for at least 2 months in patients recovered from COVID-19 (refs. [13,32]). A previous study showed that GP73 production is activated and correlated with interferon-β activation during RNA viral infection through MAVS[33]. Potential mechanisms for the regulation of GP73 expression demonstrated the involvement of cytokines, liver damage and mTOR signaling[34–36]. Therefore, GP73 expression may be

controlled in SARS-CoV-2-dependent and SARS-CoV-2-independent manners. It should be noted that HFD and HBV/HCV infection also induce circulating GP73 levels[37,38]. As a Golgi-resident protein exhibiting glucoregulatory actions, the potential contribution of GP73 to glucose abnormalities in the context of infection with other viruses, or in metabolic diseases, including diabetes, warrants further investigation. Apart from the role of GP73 in promoting cell proliferation, tumor development and metastasis, GP73 also represses the host innate immune response to
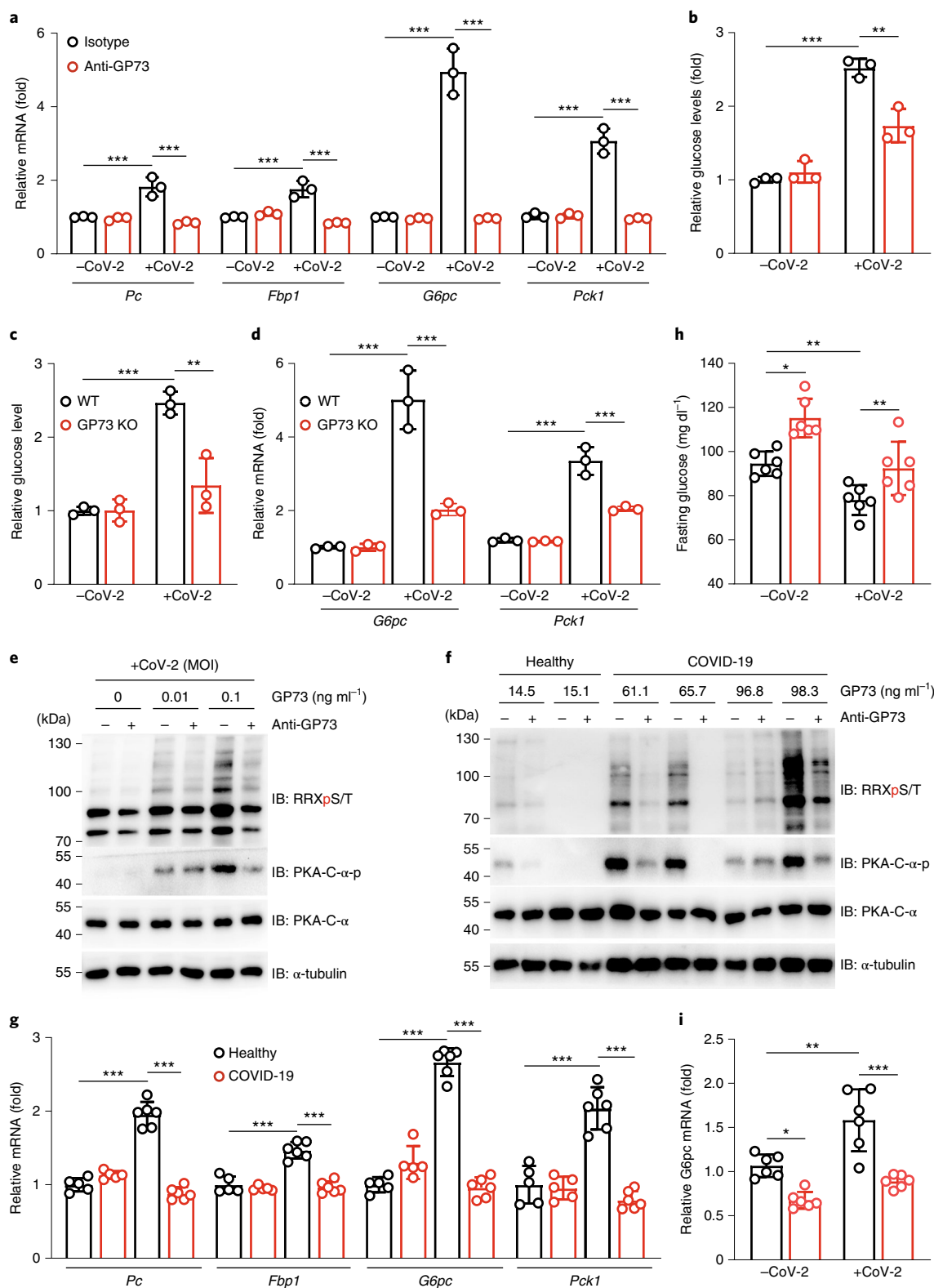
promote RNA virus replication[33,39]. Therefore, long-term follow-up of infected patients is warranted. Due to the urgent circumstance of the COVID-19 pandemic, we were unable to retrieve more clinical data including information on body mass index, steatohepatitis and fibrosis status from the current patient cohort. Although all patients were HBV, HCV and HIV negative, the possibility that NASH might have influenced GP73 release cannot be fully excluded.

In summary, we provide evidence that SARS-CoV-2 infection induces GP73 production and secretion, which results in an exaggerated gluconeogenic response. Sustained elevated GP73 may directly predispose the host to abnormal glucose metabolism (Extended Data Fig. 10). Our findings suggest that neutralizing plasma GP73 might be therapeutic option for treating patients with SARS-CoV-2 infection that warrants further investigation.

Fig. 7 | GP73 blockade inhibits SARS-CoV-2-induced gluconeogenesis enhancement. a,b, Glucogenic gene expression (**a**) or glucose levels (**b**) in Huh-7 cells infected with SARS-CoV-2 (MOI 0.1) for 24 h with or without GP73 antibody (1 µg ml⁻¹). $P = 0.0004$ for infected versus mock (*Pc*) and $P = 0.0001$ for anti-GP73 versus isotype (*Pc*, infected), $P = 0.0002$ for infected versus mock (*Fbp1*) and $P < 0.0001$ for anti-GP73 versus isotype (*Fbp1*, infected), $P < 0.0001$ for infected versus mock (*G6pc*) and $P < 0.0001$ for anti-GP73 versus isotype (*G6pc*, infected), $P < 0.0001$ for infected versus mock (*Pck1*) and $P < 0.0001$ for anti-GP73 versus isotype (*Pck1*, infected) by one-way ANOVA followed by Bonferroni's post hoc test (**a**), $P < 0.0001$ for infected versus mock and $P = 0.0013$ for anti-GP73 versus isotype by one-way ANOVA followed by Bonferroni's post hoc test (**b**). **c,d,** Glucose levels (**c**) or hepatic glucogenic gene expression (**d**) in WT and GP73 KO-1 Huh-7 cells infected with SARS-CoV-2 (MOI 0.1) for 24 h in glucose-free medium. $P = 0.0002$ for infected versus mock (WT) and $P = 0.0014$ for GP73 KO versus WT (infected) by one-way ANOVA followed by Bonferroni's post hoc test (**c**). $P < 0.0001$ for infected versus mock (*G6pc*, WT) and $P = 0.0001$ for GP73 KO versus WT (*G6pc*, infected), $P < 0.0001$ for infected versus mock (*Pck1*, WT) and $P = 0.0002$ for GP73 KO versus WT (*Pck1*, infected) by one-way ANOVA followed by Bonferroni's post hoc test (**d**). **e,f,** Immunoblotting analysis of PKA-C-α phosphorylation and substrate levels in Huh-7 cells treated with SARS-CoV-2 or the indicated serum. **g,** Glucogenic gene expression in Huh-7 cells cultured with the indicated serum with or without GP73 antibody. $P < 0.0001$ for COVID-19 versus healthy (*Pc*, *Fbp1*, *G6pc* and *Pck1*) and $P < 0.0001$ for anti-GP73 versus isotype (*Pc*, *Fbp1*, *G6pc* and *Pck1*; COVID-19) by one-way ANOVA followed by Bonferroni's post hoc test. **h,i,** Fasting glucose levels and hepatic G6pc mRNA expression in mice inoculated with 1.6×10^4 p.f.u. of MASCp6 and killed at day 2 after inoculation ($n = 6$). $P = 0.0213$ for anti-GP73 versus isotype (mock), $P = 0.0030$ for infected versus mock and $P = 0.0011$ for anti-GP73 versus isotype (infected) by one-way ANOVA followed by Bonferroni's post hoc test (**h**). $P = 0.0152$ for anti-GP73 versus isotype (mock), $P = 0.0012$ for infected versus mock and $P < 0.0001$ for anti-GP73 versus isotype (infected) by one-way ANOVA followed by Bonferroni's post hoc test (**i**). Animal and cell-based studies were performed independently at least three biological replicates with comparable results. Data are mean ± s.e.m. *$P < 0.05$; **$P < 0.01$; ***$P < 0.001$.

Methods

Reagents. Sodium L-lactate (71718), sodium pyruvate (792500) and aprotinin (A6106) were purchased from Sigma-Aldrich. Insulin (2018283062) was purchased from Novo Nordisk. Glucagon (HY-P0082) and FSK (HY-15371) were purchased from MedChemExpress. Glucose (20171108) was purchased from Sinopharm Chemical Reagent. A blood glucose meter (06656919032) and test strips (1072332990) were purchased from Roche. Sulfo-cyanine7 NHS ester (Cy7, GY1058) was purchased from Goyoo Biotechnology. Dulbecco's modified Eagle's medium (DMEM; high-glucose, D5796), protease inhibitor cocktail I (20-201) and a dipeptidyl peptidase-4 (DPP4) inhibitor (DPP4-010) were purchased from Millipore. Low-glucose DMEM (31600-500), glucose-free DMEM (90113-500) and L-alanine (A8210) were purchased from Solarbio. Fetal bovine serum (FBS; A3160901) was purchased from Gibco. Lipofectamine 2000 (11668-027) was purchased from Invitrogen. Chow (HD1001) and HFD (HD001) were purchased from BiotechHD. H89 (S1643) was purchased from Beyotime, LY2409021 (HY-19904) was purchased from MedChemExpress and cAMPS-Rp triethylammonium salt (151837-09-1) was purchased from Tocris Bioscience. Collagenase IV (2091) was purchased from BioFroxx. PerfectStart Green qPCR SuperMix (AQ601) and TransScript One-Step gDNA Removal and cDNA Synthesis SuperMix (AT311) were purchased from TransGen Biotech. NucleoZOL (740404) was purchased from MACHEREY-NAGEL. A mouse insulin ELISA kit (PI602) and BCA protein concentration determination kit (P0012) were purchased from Beyotime. A cAMP assay kit (ab133051) and PKA Kinase Activity kit (ab139435) were purchased from Abcam. An Amplex Red Glucose/Glucose Oxidase Assay kit (A22189) was purchased from Invitrogen.

Antibodies. Anti-α-tubulin (T6074, 1:5,000 dilution) and anti-Flag (A8592, 1:5,000 dilution) antibodies were purchased from Sigma-Aldrich. An anti-GP73 antibody (F-12, sc-393372, 1:200 dilution) was purchased from Santa Cruz. An anti-His antibody (KM8001, 1:1,000 dilution) was purchased from Taihua Lekang Biotechnology. Anti-phospho-PKA-C-α (Thr197, 5661, 1:1,000 dilution), anti-phospho-PKA substrate (RRXpS/T, 9624, 1:1,000 dilution) and anti-PKA-C-α (5842, 1:1,000 dilution) antibodies were purchased from Cell Signaling Technology. Anti-rabbit HRP-IgG (ZB-2301, 1:5,000 dilution) and anti-mouse HRP-IgG (ZB-2305, 1:5,000 dilution) secondary antibodies were purchased from ZSGB-BIO. Anti-spike (GTX632604, 1:500 dilution) antibody was purchased from GeneTex. An anti-GP73 monoclonal antibody for the blocking experiment was custom made. Isotype-matched IgG (A7028) was purchased from Beyotime.

Plasmids and cell culture. Mammalian expression vectors encoding Flag-tagged human, mouse and rat GP73 were constructed by inserting the corresponding PCR-amplified fragments into pcDNA3 (Invitrogen). The 23 genes of SARS-CoV-2 (Wuhan-Hu-1, GenBank, NC_045512.2) were optimized and cloned into the pXJ2 expression vector with a 3× Flag tag at the C terminus as previously described[40]. All constructs were verified by DNA sequencing. An expression plasmid for human Flag-ACE2 (H3673) was obtained from Vigene Biosciences. The HepG2 (CRL-10741), Caco-2 (HTB-37), A549 (CCL-185), Vero E6 (CRL-1586), L6 (CRL-1658) and 293T (CRL-3216) cell lines were obtained from the American Type Culture Collection. The Huh-7 (0403) cell line was obtained from the Japanese Collection of Research Bioresources. All cell lines were tested for mycoplasma contamination and were incubated in DMEM at 37 °C in a humidified atmosphere with 5% CO₂. Lipofectamine 2000 was used for transfection following the manufacturer's protocol.

To knock out human GP73 in Huh-7 cells, two small guide RNAs (sgRNAs) targeting GP73 were designed and inserted into the LentiCrispr v2 vector to construct transfer plasmids. 293T cells were transfected with pMD2. G, psPAX2 and the corresponding transfer plasmid to produce lentivirus. A total of 10^8 Huh-7 cells were infected with lentivirus at an MOI of 2.0 and selected with 4 µg ml⁻¹ puromycin for 2 weeks to ensure proper selection.

The following sgRNA sequences were used:
sgRNA-1: 5′-CACCGCACACACAGAGGTGCCACAA-3′
sgRNA-2: 5′-CACCGACCAGTTAAAGACCCTGCAG-3′
control- 5′-CACCGCGCTTCCGCGGCCCGTTCAA-3′.

PMHs were isolated and purified using a modified two-step collagenase perfusion method. Cells were resuspended in low-glucose DMEM containing 5% FBS and seeded on 15-cm dishes at 80% confluence. Five hours later, the cells were washed and cultured in serum-free medium overnight. For gluconeogenesis-related assays, the medium was replaced with glucose-free and phenol-free DMEM the next day in the presence of 10 mM pyruvate sodium and 10 mM sodium lactate and the cells were treated with the indicated concentrations of rmGP73 or rrGP73, 200 mM cAMPS-Rp or 2 µM glucagon.

Sample acquisition from patients with COVID-19. The Ethics Committee of Huoshenshan Hospital approved the study (HSSLL036). Given the urgency of the COVID-19 pandemic, the need for informed consent forms was waived by the ethics boards of the hospitals. Basic information, serum biochemical test results and blood samples for GP73 and glucose level analysis were collected from 76 patients with COVID-19 at Huoshenshan Hospital from 11 January to 11 March 2020 at admission before any intervention. Diagnosis was based on chest computed tomography (CT) manifestations and/or PCR with reverse transcription (RT–PCR) according to the criteria of the New Coronavirus Pneumonia Prevention and Control Program (5th edition) published by the National Health Commission of China. According to these criteria, patients with COVID-19 were classified into mild, moderate and severe COVID-19 subgroups. The majority of patients received combined treatments, including antiviral drugs (lopinavir/ritonavir, interferon-α and arbidol), herbs, intravenous immunoglobulin and antibiotics. Data were excluded if the patient was younger than 18 years or older than 75 years, had incomplete medical records, acute lethal organ injury (for example, acute myocardial infarction, acute coronary syndrome, acute pulmonary embolism or acute stroke) or decompensated/end-stage chronic organ dysfunction (for example, decompensated cirrhosis, decompensated chronic renal insufficiency or severe congestive heart failure), was pregnant, was HBV-, HCV- or HIV-positive, used drugs with known effects on glucose metabolism (glucocorticoid or tocilizumab) or had malignancy (Supplementary Table 1). Twenty-eight patients had mild COVID-19, 36 patients had moderate COVID-19 and 12 patients had severe COVID-19 (Supplementary Table 2). Among them, four patients with moderate COVID-19 and nine patients with severe COVID-19 were enrolled and blood samples were collected at admission before any intervention, during hospitalization and after recovery before discharge. The discharge criteria included normal temperature, resolved respiratory symptoms, improved CT images and two consecutively negative RT–PCR results for SARS-CoV-2 in respiratory tract specimens within an interval of at least 24 h.

Recombinant GP73 protein purification. Human, mouse and rat GP73 complementary DNAs, each with a six-amino-acid His tag on the N terminus, were cloned into the pCDNA3.1 vector. Ni-NTA His-Bind column-bound His-GP73 protein from 293T cells transfected with the above plasmids was further purified

using size-exclusion columns and polymyxin B-based endotoxin-depletion columns after extensive washing. The final His-GP73 proteins used in all recombinant protein experiments were >90% pure (endotoxin ≤2 EU ml⁻¹) and stored at −80 °C.

Animals, intervention and monitoring. Male C57BL/6N WT mice (8–10 weeks old) were purchased from SPF Biotechnology. Male GP73 KO mice (T20200316-18[D25], 8–10 weeks old) were generated from C57BL/6N WT mice by Southern Model Biotechnology. All mice were group-housed conventionally on a 12-h light/dark cycle for 3 d before any experiments, the environmental conditions were maintained thermostatically between 18 °C −23 °C with 40–60% humidity. All animal experiments were performed at the AMMS Animal Center and were approved by the Institutional Animal Care and Use Committee. For single injection, mice were injected i.v. with 0.1 mg kg⁻¹ rmGP73 and plasma was collected at the indicated times via tail bleeding for insulin and glucose level measurements. The ITT, GTT, PTT and ATT were performed using standard procedures. A 0.75 U kg⁻¹ insulin bolus was used for the ITT, a 1.5 g kg⁻¹ glucose bolus was used for the GTT, a 1.5 g kg⁻¹ pyruvate bolus was used for the PTT and a 0.6 g kg⁻¹ alanine bolus was used for the ATT. For immunological sequestration experiments, mice were injected i.v. with 15 mg kg⁻¹ custom-made anti-GP73 mouse monoclonal antibody or an equivalent dose of IgG (30 mg kg⁻¹).

Glucose measurement. All blood samples were collected from the tail and glucose levels were measured using the glucose oxidase method and an automated blood glucose reader (ACCU-CHEK, Roche). For the measurement of fasting blood glucose levels, normal mice were fasted for 6 or 12 h as indicated. Random blood glucose levels were measured at 9:00 a.m. If the glucose level was >630 mg dl⁻¹ (upper detection limit of the glucometer), a value of 630 mg dl⁻¹ was recorded. Blood glucose levels were determined.

Assays of plasma hormone levels. Blood samples for hormone detection were collected from the tail or orbital vein. A DPP4 inhibitor (1:100 dilution), aprotinin (1:100 dilution) and protease inhibitor cocktail I (50,000 KIU ml⁻¹, 1:100 dilution) were added to each blood sample. Plasma insulin levels were measured using ELISA.

Hyperinsulinemic-euglycemic clamp. The assays were performed as previously described[41]. Mice were anesthetized with an intraperitoneal injection of 50 mg kg⁻¹ pentobarbital sodium salt (Sigma, P3761). Hairs at the incision site were removed by an electric hair clipper. An incision was made in the skin and the right jugular vein was identified. A catheter (Instech Laboratories, C10PU-MCA1301) filled with heparinized saline (200 U heparin per ml saline) was inserted into the vein toward the side of the chest. A suture was placed at each end of the vessel. The catheter was tunneled under the skin from the right jugular to the interscapular incision on the back. The catheter was plugged with a mouse button harness (Instech Laboratories, VABM2B/22R22) and settled on the back. All skin wounds were sutured and the mouse recovered for 3–4 d. Mice that lost <5% of their precannulation weight after recovery were used for clamp studies.

The mice were fasted overnight, weighed to calculate the insulin dose and placed in a transparent plastic terrarium (Instech Laboratories, STANK/W). The setup and timeline for the experiment are shown in Extended Data Fig. 6a. An equilibration syringe pump was connected to the catheter and GFP or GP73 was administered at $t = -150$ min. At $t = -90$ min, [6,6-²H] glucose (600 μg kg⁻¹) was administered, followed by continuous infusion of [6,6-²H] glucose (30 μg kg⁻¹ min⁻¹). Isotopic enrichment was achieved at approximately 60 min after the onset of isotope infusion and blood samples for isotope measurements were collected at $t = -10$ and 0 min. Following this basal infusion period, insulin was constantly infused at a rate of 6 mU kg⁻¹ min⁻¹ until termination of the study. [6,6-²H]glucose was infused together with glucose at various rates until the blood glucose concentration reached a constant level of approximately 100 ± 10 mg dl⁻¹. Blood samples were taken at $t = 110$ and 120 min.

Mass spectrometry. Mass spectrometry was performed at the Protein Preparation and Characterization Platform of the Tsinghua University Technology Center for Protein Research as previously described[41]. Plasma samples (15 μl) were deproteinized by gently mixing them with 60 μl cold methanol (prechilled at −80 °C) and incubating for 1–2 h at −80 °C. The samples were then centrifuged at 14,000g at 4 °C for 10 min. The supernatant was transferred to a new tube and lyophilized to produce a pellet. High-resolution mass spectrometry (Q ExactiveHFX, Thermo) coupled with Vanquish UHPLC was used for the analysis. Negative ion mode with a mass resolution of 120,000 was performed for glucose detection. The flow rates of sheath gas and aux gas were set as 35 and 10, respectively. Spray voltage was 2.8 kV. For LC separation, an amide column (2.1 mm × 100 mm, Waters) was used for analysis of glucose. Column temperature was 40 °C. Mobile phases contained 80% acetonitrile in A and 30% acetonitrile in B with 5 mM ammonium acetate as a modifier. The flow rate was 250 μl min⁻¹ and the gradient was as follows: 0–3 min: 10% B; 3–4 min: 10–60% B; 4–6 min: 60% B; 6.1–8 min: 10% B. A total of 2 μl of sample was injected for analysis. Accurate masses of 179.0561 and 181.0686 with a mass tolerance of 3 ppm were used for the

extraction of glucose and [6,6-²H]glucose in negative mode. For the calibration curve, concentrations of 5, 10, 25, 50, 100, 250, 500, 1,000, 2,500, 5,000, 10,000, 25,000 ng ml⁻¹ for [6,6-²H]glucose and 1, 2, 5, 10, 20, 50, 100, 200, 500, 1,000, 2,500, 5,000 μg ml⁻¹ for glucose were prepared in 80% methanol.

Calculation. All calculations are based on Steele's equations for steady-state conditions[41,42]. Under steady-state conditions, the rate of glucose appearance (Ra) is equal to the rate of disappearance (Rd)[43]. The GDR is equal to the constant isotope infusion rate (F) divided by isotope enrichment (atom percent excess, APE) minus F. There is no glucose infusion during the basal infusion period, so GDR is equal to the rate of HGP. During infusion of unlabeled glucose mixed with [6,6-²H] glucose, GDR is equal to the sum of the rate of HGP and the glucose infusion rate (GIR). The HGP is equal to GDR minus GIR. The calculation was performed as indicated in Extended Data Fig. 6b.

Immunofluorescence staining. Tissues were fixed with 10% (v/v) neutral-buffered formalin at 4 °C overnight and embedded in paraffin and 5-μm-thick sections were prepared. For immunofluorescence, the sections were heated in an autoclave in citrate buffer (12 mmol l⁻¹, pH 6.0), preincubated in permeabilization/blocking buffer (0.1 mmol l⁻¹ PBS, pH 7.3, 0.5% Triton) and blocked for 30 min with 10% (v/v) goat serum (Zhongshan Biotechnology). The sections were subsequently incubated with primary antibodies at 4 °C overnight and secondary antibodies for 1 h at room temperature, washed and stained with 4,6-diamidino-2-phenylindole (1 μg ml⁻¹). Images were captured under a confocal fluorescence microscope (Zeiss LSM710, Carl Zeiss Microscopy) or an automatic digital slide scanner (Pannoramic MIDI, 3D HISTECH). Nikon NIS-Elements AR 4.00.12 and CaseViewer 2.4 software were used to analyze the image data.

Phosphoproteomics. PMHs were suspended in low-glucose DMEM containing 5% FBS and seeded in 15-cm dishes at 80% confluence. Cells were washed and cultured in serum-free medium overnight 5 h later. The medium was replaced with glucose-free and phenol-free DMEM supplemented with 10 mM pyruvate sodium and 10 mM sodium lactate the next day and the cells were incubated for 1 h with PBS, rmGP73 (64 nM) or glucagon (2 μM). For cell lysate collection, the cells were washed twice with cold PBS and scraped with cold RIPA lysis buffer supplemented with protease and phosphatase inhibitors. Phosphoproteomics was performed by Oebiotech Company. Briefly, samples were subjected to enzyme digestion and iTRAQ labeling and the phosphopeptides were enriched and analyzed using LC–MS/MS. The raw data of this study have been deposited in the IProX database under accession no. PXD025381. For kinase enrichment, the Literature Based Kinase–Substrate Library with Phosphosites on the Kinase Enrichment Analysis 2 (KEA2) website was searched (https://www.maayanlab.net/KEA2/). The network was represented using Cytoscape v.3.6.2 (https://cytoscape.org/). Protein–protein interactions were retrieved from STRING App (v.1.51) (https://string-db.org/). Only interactions with high confidence (interaction score >0.7) from databases and experiences were kept. For KEGG and Gene Ontology enrichment analysis, DAVID Bioinformatics Resources 6.8 (https://david.ncifcrf.gov/home.jsp) was used. For specific kinase–substrate motif analysis, MoMo Modification Motifs 5.3.3 (https://meme-suite.org/tools/momo) was used.

In vivo imaging system. GP73 was labeled with Cy7 via the addition of the dye according to the manufacturer's instructions at pH 8.0 and incubation of the mixture for 4 h on ice. Labeled GP73 was returned to pH 7.0 and the free dye was removed via overnight dialysis in PBS. The labeled GP73 was added to a Sephadex G50 size-exclusion column equilibrated with PBS. Fractions of 500 μl were collected, the protein concentration was analyzed using a standard BCA protein assay kit and fluorescence corresponding to excitation/emission of 745/800 nm was assessed.

After i.v. injection with free Cy7 and GP73-Cy7, mice were scanned using an IVIS (PerkinElmer) at the indicated time points to assess fluorescence. After whole-body imaging, the mice were sacrificed and the major organs were imaged to assess fluorescence under the same settings as the in vivo imaging. The data were analyzed and exported using built-in Living Image Software (v.4.5.5, PerkinElmer).

Quantitative real-time PCR. Total mRNA was extracted from cells or various mouse tissues using NucleoZOL. cDNA was prepared from total mRNA using TransScript One-Step gDNA Removal and cDNA Synthesis SuperMix and the relative levels of individual mRNAs were calculated after normalization to the GAPDH mRNA level in the corresponding sample as previously described. Primer sequences are presented in Supplementary Table 3.

Sandwich ELISA and western blot analysis. For GP73 sandwich ELISA, two custom-made rat monoclonal anti-GP73 antibodies were used as the capture antibody and the detection antibody. Briefly, the plate was coated with an unlabeled capture antibody and serially diluted standards and samples were added to the plate. After three washes, HRP-linked detection antibody was added to generate a colorimetric signal at 450 nm. Increasing amounts of recombinant His-tagged GP73 were used to generate a standard curve.

For immunoblotting, cells were lysed in NP40 cell lysis buffer with fresh protease inhibitors. Whole-cell lysates were separated using SDS–PAGE after centrifugation and transferred to polyvinylidene difluoride membranes for immunoblot analyses using the indicated primary antibodies.

Infection with SARS-CoV-2. All procedures involving cells and animals were conducted in the Biosafety Level 3 laboratory (BSL-3) and approved by the Animal Experiment Committee of Laboratory Animal Center, Beijing Institute of Microbiology and Epidemiology (approval number: IACUC-DWZX2020-002). Animal studies were carried out in strict accordance with the recommendations in the Guide for the Care and Use of Laboratory Animals.

The SARS-CoV-2 strain (BetaCoV/Beijing/IME-BJ01/2020) used for cell infection in the present study was isolated from the lung lavage fluid of an infected patient and preserved at the State Key Laboratory of Pathogen and Biosecurity at Beijing Institute of Microbiology and Epidemiology. The infectious virus titer was determined as p.f.u. in Vero E6 cells and was used to calculate the MOI. Cells were infected with SARS-CoV-2 at the indicated MOIs for the indicated times in glucose-free medium for the production assay. The results were normalized to the protein content. Cells were infected with SARS-CoV-2 at the indicated MOIs for the indicated time and the supernatant was collected for the GP73 assay and viral load assay. Viral RNA was extracted from supernatants using the QIAamp Viral RNA Mini kit (52906, QIAGEN) according to the manufacturer's instructions. Viral RNA was analyzed using qRT–PCR and a One-Step PrimeScript RT–PCR kit (RR064B, TaKaRa) using SARS-CoV-2-specific primers in an Applied Biosystems 7500 Real-time PCR System. The following sequences of the SARS-CoV-2 probes were used:

SARS-CoV-2 open reading frame 1b (ORF1b):
Forward: 5′- CCCTGTGGGTTTTACACTTAA-3′
Reverse: 5′- ACGATTGTGCATCAGCTGA-3′.
Probe: 5′-FAM- CCGTCTGCGGTATGTGGAAAGGTTATGG-BHQ 1-3′.
SARS-CoV-2 nucleocapsid (N):
Forward: 5′- GGGGAACTTCTCCTGCTAGAAT-3′
Reverse: 5′- CAGACATTTTGCTCTCAAGCTG-3′.
Probe: 5′-FAM- TTGCTGCTGCTTGACAGATT-BHQ 1-3′.

The number of copies per µl was determined using a synthetic RNA fragment to amplify the target region.

The mouse-adapted SARS-CoV-2 strain MASCp6 used for mouse infection in the present study was from the Beijing Institute of Microbiology and Epidemiology and was stored at −80 °C. Nine-month-old male BALB/c mice were inoculated intranasally with MASCp6 (6×10^3 p.f.u. per mouse). For the measurement of fasting blood glucose levels, infected mice were fasted for 6 h on day 2 after infection, blood samples were collected from the tail and glucose levels were measured as uninfected mice. For mice samples collection, the sera were collected and mice were killed. Lung and liver tissues were subjected to viral RNA load analysis and immunohistochemistry analysis for GP73. Copies per ml were determined using a synthetic RNA fragment to amplify the target region.

Pseudovirus production. All pseudoparticles were generated in 293T cells transfected with the HIV backbone vector pNL4-3.Luc. R-E together with the plasmids encoding SARS-2-S or VSV-G as previously described.

Statistical analysis. Microsoft Office Standard 2010 was used for data calculation and GraphPad Prism 8.0 was used for statistical calculations and data plotting. Data are presented as mean ± s.e.m. Differences between two independent samples were evaluated using two-tailed Student's t-tests or the Mann–Whitney U-test, as appropriate. Differences between multiple samples were analyzed using one-way or two-way ANOVA followed by Bonferroni's post hoc test, as appropriate. Correlations were analyzed using Spearman's nonparametric test. All tests were two-tailed unless otherwise indicated. We considered a P value ≤ 0.05 to be statistically significant. Significance values were set as follows: NS, not significant, $P > 0.05$; *$P < 0.05$; **$P < 0.01$; and ***$P < 0.001$.

Data availability

The numeric source data are provided in source data files and all of the other data that support the findings of this study are available from the corresponding author upon reasonable request. The phosphoproteomics data have been deposited in iProX database and are accessible through accession number PXD025381. All online datasets used in this study including KEGG (https://www.genome.jp/kegg/), DAVID (https://david.ncifcrf.gov/home.jsp), Cytoscape (https://cytoscape.org/) MoMo (https://meme-suite.org/tools/momo), STRING (https://string-db.org/) and KEA2 (https://www.maayanlab.net/KEA2/). Source data are provided with this paper.

References

1. Roder, P. V., Wu, B., Liu, Y. & Han, W. Pancreatic regulation of glucose homeostasis. *Exp. Mol. Med* **48**, e219 (2016).
2. Sharabi, K., Tavares, C. D., Rines, A. K. & Puigserver, P. Molecular pathophysiology of hepatic glucose production. *Mol. Asp. Med.* **46**, 21–33 (2015).
3. Chadt, A. & Al-Hasani, H. Glucose transporters in adipose tissue, liver, and skeletal muscle in metabolic health and disease. *Pflug. Arch.* **472**, 1273–1298 (2020).
4. Kowalski, G. M. & Bruce, C. R. The regulation of glucose metabolism: implications and considerations for the assessment of glucose homeostasis in rodents. *Am. J. Physiol. Endocrinol. Metab.* **307**, E859–E871 (2014).
5. Chung, S. T., Chacko, S. K., Sunehag, A. L. & Haymond, M. W. Measurements of gluconeogenesis and glycogenolysis: a methodological review. *Diabetes* **64**, 3996–4010 (2015).
6. Zhang, X., Yang, S., Chen, J. & Su, Z. Unraveling the regulation of hepatic gluconeogenesis. *Front. Endocrinol.* **9**, 802 (2018).
7. Fleig, W. E., Noether-Fleig, G., Roeben, H. & Ditschuneit, H. Hormonal regulation of key gluconeogenic enzymes and glucose release in cultured hepatocytes: effects of dexamethasone and gastrointestinal hormones on glucagon action. *Arch. Biochem. Biophys.* **229**, 368–378 (1984).
8. Deng, L. et al. Hepatitis C virus infection promotes hepatic gluconeogenesis through an NS5A-mediated, FoxO1-dependent pathway. *J. Virol.* **85**, 8556–8568 (2011).
9. Petersen, M. C., Vatner, D. F. & Shulman, G. I. Regulation of hepatic glucose metabolism in health and disease. *Nat. Rev. Endocrinol.* **13**, 572–587 (2017).
10. Cristelo, C., Azevedo, C., Marques, J. M., Nunes, R. & Sarmento, B. SARS-CoV-2 and diabetes: new challenges for the disease. *Diabetes Res Clin. Pr.* **164**, 108228 (2020).
11. Lim, S., Bae, J. H., Kwon, H. S. & Nauck, M. A. COVID-19 and diabetes mellitus: from pathophysiology to clinical management. *Nat. Rev. Endocrinol.* **17**, 11–30 (2021).
12. Sathish, T. & Chandrika Anton, M. Newly diagnosed diabetes in patients with mild to moderate COVID-19. *Diabetes Metab. Syndr.* **15**, 569–571 (2021).
13. Montefusco, L. et al. Acute and long-term disruption of glycometabolic control after SARS-CoV-2 infection. *Nat. Metab.* **3**, 774–785 (2021).
14. Ayres, J. S. A metabolic handbook for the COVID-19 pandemic. *Nat. Metab.* **2**, 572–585 (2020).
15. Alves, A. M., Yvamoto, E. Y., Marzinotto, M. A. N., Teixeira, A. C. S. & Carrilho, F. J. SARS-CoV-2 leading to acute pancreatitis: an unusual presentation. *Braz. J. Infect. Dis.* **24**, 561–564 (2020).
16. Liu, F. et al. ACE2 expression in pancreas may cause pancreatic damage after SARS-CoV-2 infection. *Clin. Gastroenterol. Hepatol.* **18**, 2128–2130 (2020).
17. Muller, J. A. et al. SARS-CoV-2 infects and replicates in cells of the human endocrine and exocrine pancreas. *Nat. Metab.* **3**, 149–165 (2021).
18. Kladney, R. D. et al. GP73, a novel Golgi-localized protein upregulated by viral infection. *Gene* **249**, 53–65 (2000).
19. Hu, L., Li, L., Xie, H., Gu, Y. & Peng, T. The Golgi localization of GOLPH2 (GP73/GOLM1) is determined by the transmembrane and cytoplamic sequences. *PLoS ONE* **6**, e28207 (2011).
20. Puri, S., Bachert, C., Fimmel, C. J. & Linstedt, A. D. Cycling of early Golgi proteins via the cell surface and endosomes upon lumenal pH disruption. *Traffic* **3**, 641–653 (2002).
21. Wei, C. et al. Tumor microenvironment regulation by the endoplasmic reticulum stress transmission mediator Golgi protein 73 in mice. *Hepatology* **70**, 851–870 (2019).
22. Wang, L. et al. Serum Golgi protein 73 as a potential biomarker for hepatic necroinflammation in population with nonalcoholic steatohepatitis. *Dis. Markers* **2020**, 6036904 (2020).
23. Nie, X. et al. Multi-organ proteomic landscape of COVID-19 autopsies. *Cell* **184**, 775–791 (2021).
24. Gu, H. et al. Adaptation of SARS-CoV-2 in BALB/c mice for testing vaccine efficacy. *Science* **369**, 1603–1607 (2020).
25. Romere, C. et al. Asprosin, a fasting-induced glucogenic protein hormone. *Cell* **165**, 566–579 (2016).
26. Yabaluri, N. & Bashyam, M. D. Hormonal regulation of gluconeogenic gene transcription in the liver. *J. Biosci.* **35**, 473–484 (2010).
27. Perry, R. J. et al. Glucagon stimulates gluconeogenesis by INSP3R1-mediated hepatic lipolysis. *Nature* **579**, 279–283 (2020).
28. Rubino, F. et al. New-onset diabetes in Covid-19. *N. Engl. J. Med.* **383**, 789–790 (2020).
29. Hollstein, T. et al. Autoantibody-negative insulin-dependent diabetes mellitus after SARS-CoV-2 infection: a case report. *Nat. Metab.* **2**, 1021–1024 (2020).
30. Hussain, A., Bhowmik, B. & do Vale Moreira, N. C. COVID-19 and diabetes: knowledge in progress. *Diabetes Res Clin. Pr.* **162**, 108142 (2020).
31. Govender, N., Khaliq, O. P., Moodley, J. & Naicker, T. Insulin resistance in COVID-19 and diabetes. *Prim. Care Diabetes* **15**, 629–634 (2021).
32. Yang, J. K., Lin, S. S., Ji, X. J. & Guo, L. M. Binding of SARS coronavirus to its receptor damages islets and causes acute diabetes. *Acta Diabetol.* **47**, 193–199 (2010).

33. Zhang, X. et al. GP73 represses host innate immune response to promote virus replication by facilitating MAVS and TRAF6 degradation. *PLoS Pathog.* **13**, e1006321 (2017).

34. Chen, X. et al. mTORC1 up-regulates GP73 to promote proliferation and migration of hepatocellular carcinoma cells and growth of xenograft tumors in mice. *Gastroenterology* **149**, 741–752 (2015).

35. Liang, H. et al. Interleukin-6 and oncostatin M are elevated in liver disease in conjunction with candidate hepatocellular carcinoma biomarker GP73. *Cancer Biomark.* **11**, 161–171 (2012).

36. Liu, X. et al. Golgi protein 73(GP73), a useful serum marker in liver diseases. *Clin. Chem. Lab. Med.* **49**, 1311–1316 (2011).

37. Kladney, R. D., Cui, X., Bulla, G. A., Brunt, E. M. & Fimmel, C. J. Expression of GP73, a resident Golgi membrane protein, in viral and nonviral liver disease. *Hepatology* **35**, 1431–1440 (2002).

38. Wolf, M. J. et al. Metabolic activation of intrahepatic CD8+ T cells and NKT cells causes nonalcoholic steatohepatitis and liver cancer via cross-talk with hepatocytes. *Cancer Cell* **26**, 549–564 (2014).

39. Wang, Y. & Wan, Y. Y. Golgi protein 73, hepatocellular carcinoma and other types of cancers. *Liver Res.* **4**, 161–167 (2020).

40. Zhang, J. et al. A systemic and molecular study of subcellular localization of SARS-CoV-2 proteins. *Signal Transduct. Target Ther.* **5**, 269 (2020).

41. Zhang, Y., Xu, L., Liu, X. & Wang, Y. Evaluation of insulin sensitivity by hyperinsulinemic-euglycemic clamps using stable isotope-labeled glucose. *Cell Discov.* **4**, 17 (2018).

42. Hother-Nielsen, O. & Beck-Nielsen, H. On the determination of basal glucose production rate in patients with type 2 (non-insulin-dependent) diabetes mellitus using primed-continuous 3-3H-glucose infusion. *Diabetologia* **33**, 603–610 (1990).

43. Radziuk, J. & Lickley, H. L. The metabolic clearance of glucose: measurement and meaning. *Diabetologia* **28**, 315–322 (1985).

Author contributions

X.Y., C.Q., Z.S., F.W., C. Wei and H.Z. designed the experiments. C. Wei, H.Z., L.W., Q.G., G.C., E.M., X.Y. and H. Li collected and analyzed data. L.W., H.Y., H. Lin, J.G., Y.K., X.Y., L.H., Jing Liu, Y.X., Jingfei Li, C.L., F.Z., J.F., Q Yan, M.L. and Y.Z. carried out mice assays. Y.D., X.H., Q.C. and Q. Ye carried out authentic virus assays. L.W., E.M., H. Lin, C. Wang, Dongyu Li, H.W., L.X., Jialong Liu, X.Z., Y.Z., Dongrui Li, M.W., Y.M., K.T., Y.Y., Jianmin Li and H.H. carried out cell lines experiments. P.W. provided key experiment materials. X.Y., L.W., C. Wei and H.Z. analyzed the data and prepared the manuscript.

Competing interests

The authors declare no competing interests.

Additional information

Extended data is available for this paper at https://doi.org/10.1038/s42255-021-00508-2.

Supplementary information The online version contains supplementary material available at https://doi.org/10.1038/s42255-021-00508-2.

Correspondence and requests for materials should be addressed to Hui Zhong.

Peer review information *Nature Metabolism* thanks John Nicholls, C. Ronald Kahn and the other, anonymous, reviewers for their contribution to the peer review of this work. Primary handling editor: Christoph Schmitt.

Reprints and permissions information is available at www.nature.com/reprints.

Publisher's note Springer Nature remains neutral with regard to jurisdictional claims in published maps and institutional affiliations.

a

b
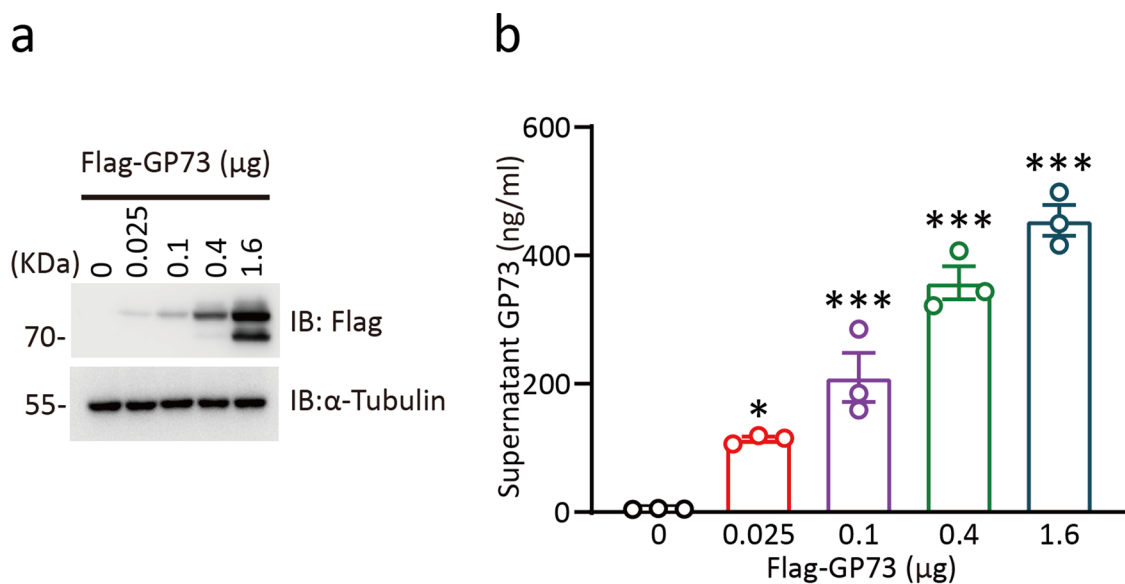
Extended Data Fig. 1 | GP73 secretion is induced from multiple tissues upon fasting. a-b, Intracellular GP73 (a) or supernatant GP73 levels (b) in HepG2 cells transfected with different concentrations of Flag-GP73. Cell-based studies were performed independently at least three times with comparable results. $P = 0.0327$ for 0.025 μg versus 0 μg, $P < 0.0001$ for 0.1 μg versus 0 μg, 0.4 μg versus 0 μg and 1.6 μg versus 0 μg by one-way ANOVA followed by Bonferroni's post hoc test. Cell-based studies were performed independently at least three times with comparable results. The data were the means ± SEMs. *$P < 0.05$, ***$P < 0.001$.
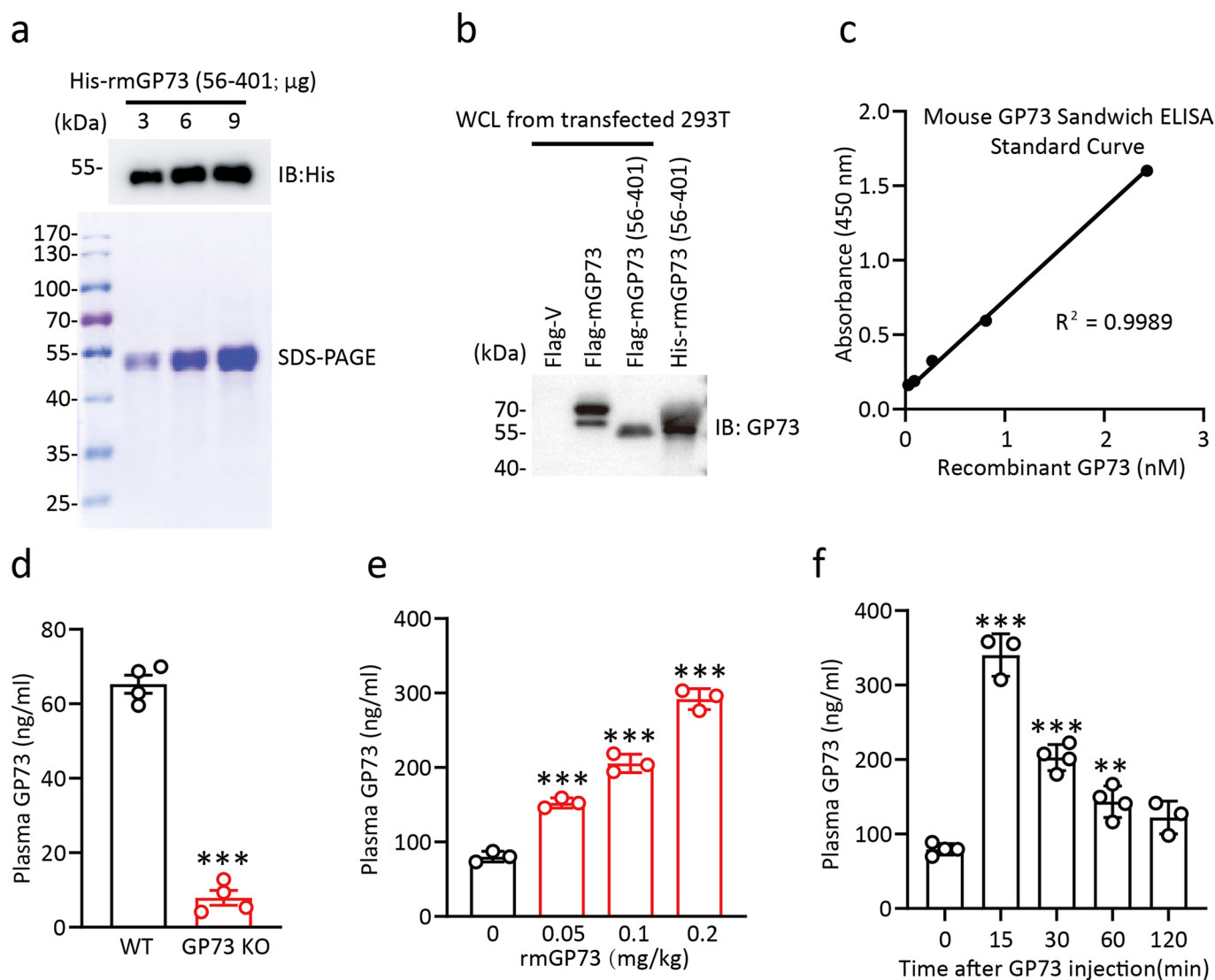
Extended Data Fig. 2 | Increase in circulating GP73 elevates fasting blood glucose. a, Immunoblotting analysis (upper lane) and SDS-PAGE (lower lane) of purified His-tagged rmGP73 (56–401). **b** Immunoblotting analysis of purified His-tagged rmGP73 (56–401) and GP73 expression in 293 T cells transfected with the indicated plasmids. **c**, Mouse sandwich ELISA standard curve. **d**, Plasma GP73 levels in WT and GP73 KO mice ($n = 4$). $P < 0.0001$ for GP73 KO versus WT by two-tailed Student's t-tests. **e-f**, Plasma GP73 levels in mice after rmGP73 injection at the indicated doses (e) for the indicated times ($n = 3$ or 4; f). $P < 0.0001$ for 0.2 mg/kg versus 0 mg/kg, 0.1 mg/kg versus 0 mg/kg and 0.05 mg/kg versus 0 mg/kg by one-way ANOVA followed by Bonferroni's post hoc test (e). $P < 0.0001$ for 15 min versus 0 min, $P < 0.0001$ for 30 min versus 0 min, $P = 0.0021$ for 60 min versus 0 min by one-way ANOVA followed by Bonferroni's post hoc test (f). Animal and cell-based studies were performed independently at least three times with comparable results. The data were the means ± SEMs. ***$P < 0.01$, ***$P < 0.001$.
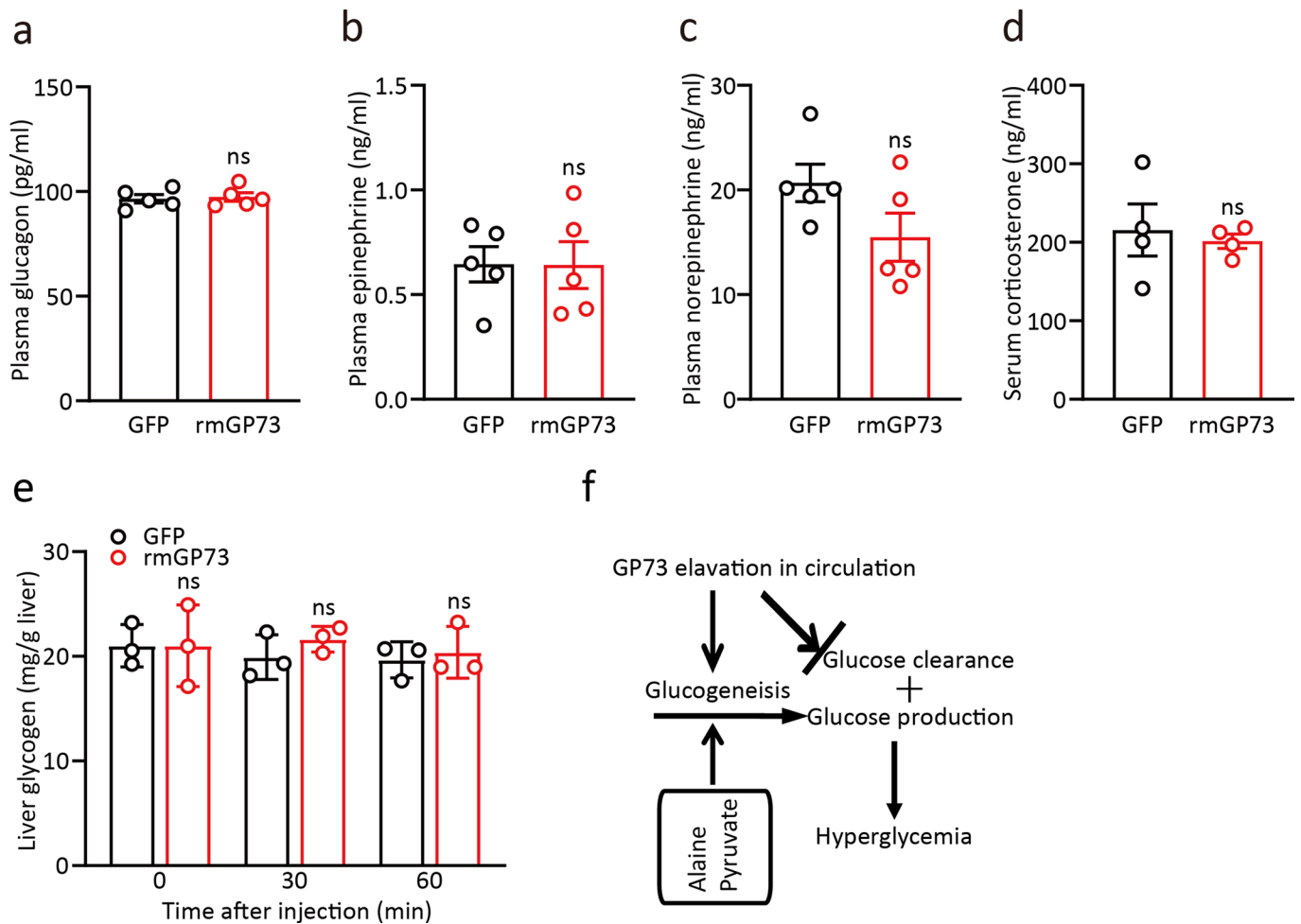
Extended Data Fig. 3 | Increase in circulating GP73 elevates fasting blood glucose. a-d, Plasma glucagon (a), epinephrine (b), norepinephrine (c) and serum corticosterone (d) levels 15 min after rmGP73 or GFP injection (n = 3 or 4). ns, no significant for rmGP73 versus GFP by two-tailed Student's t-tests (a-d). **e**, Glycogen levels in mice at 30 and 60 min after rmGP73 or GFP injection (n = 3 in each group). ns, no statistical significance for rmGP73 versus GFP (0 min, 30 min and 60 min) by two-tailed Student's t-tests (a-d). **f**, Schematic representation of the metabolic process responsible for GP73-induced hyperglycemia. Animal studies were performed independently at least three times with comparable results. The data were presented as the means ± SEMs. ns, no statistical significance.
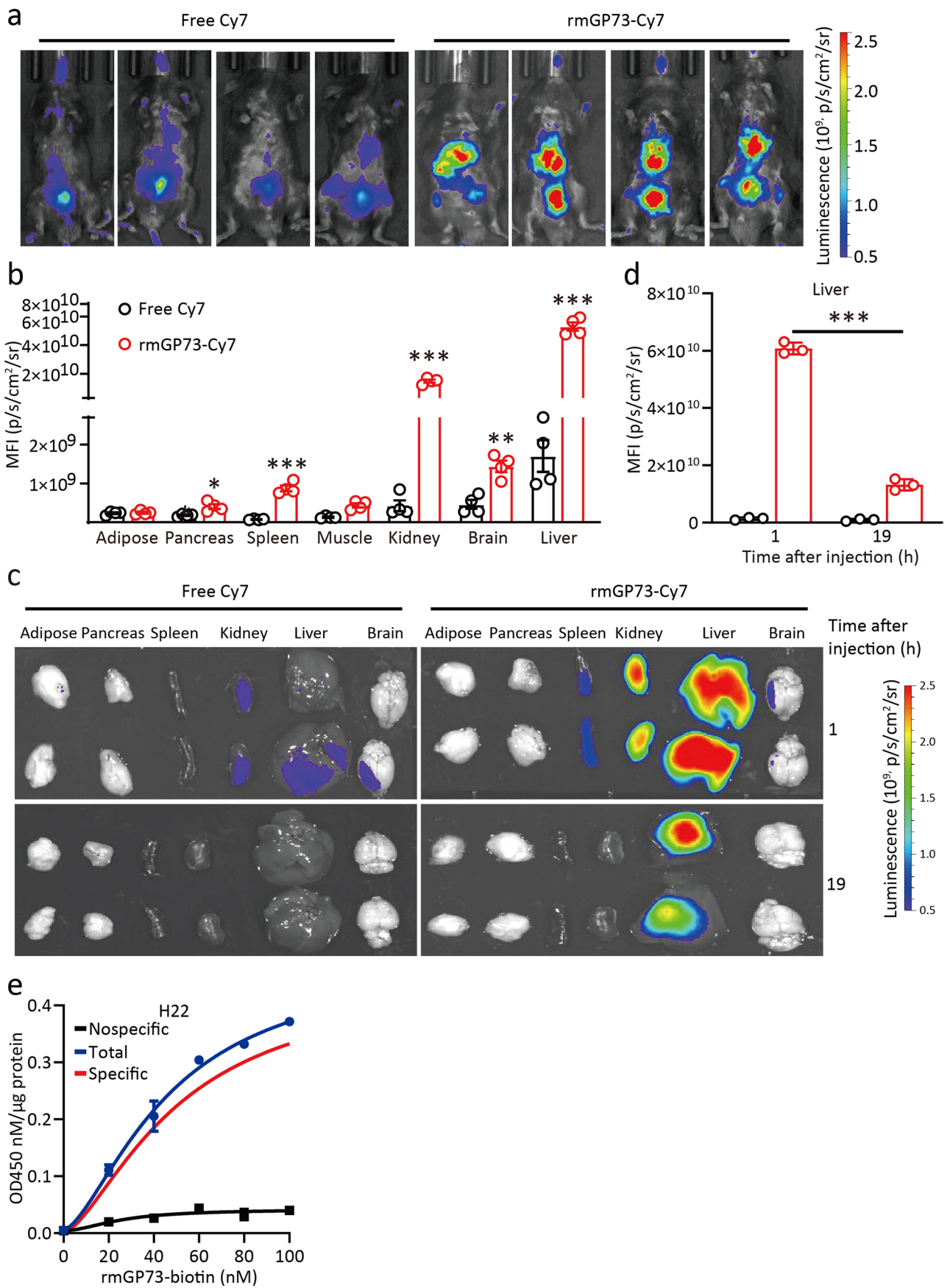
Extended Data Fig. 4 | See next page for caption.

Extended Data Fig. 4 | Circulating GP73 traffics to the liver and binds to the hepatocyte surface. a, In vivo imaging of live anesthetized mice 30 min after i.v. injection of rmGP73-Cy7 or free Cy7 (n = 4). **b**, Tissue GP73 accumulation in Fig. 3a was measured as the photon intensity. $P = 0.0129$ for rmGP73-Cy7 versus free Cy7 (pancreas), $P = 0.0019$ for rmGP73-Cy7 versus free Cy7 (brain), $P < 0.0001$ for rmGP73-Cy7 versus free Cy7 (spleen, kidney and liver) by two-tailed Student's t-tests. **c**, In vivo imaging of various organs from mice 1 h or 19 h after rmGP73-Cy7 or free Cy7 injection. Two representative images from four mice are shown. **d**, Liver GP73 accumulation in mice 1 h or 19 h after rmGP73-Cy7 or free Cy7 injection. $P < 0.0001$ for 1 h versus 19 h (rmGP73-Cy7) by one-way ANOVA followed by Bonferroni's post hoc test. **e**, The level of biotin on the hepatocyte surface upon incubation of H22 cells with increasing concentrations of rhGP73-biotin or rmGP73-biotin with (nonspecific binding) or without (total binding) 100-fold excess recombinant GP73 in the medium was measured using a colorimetric assay. Specific binding (shown in red) was calculated as the difference between the two curves. Animal and cell-based studies were performed independently at least three times with comparable results. The data were the means ± SEMs. $*P < 0.05$; $**P < 0.01$; $***P < 0.001$.
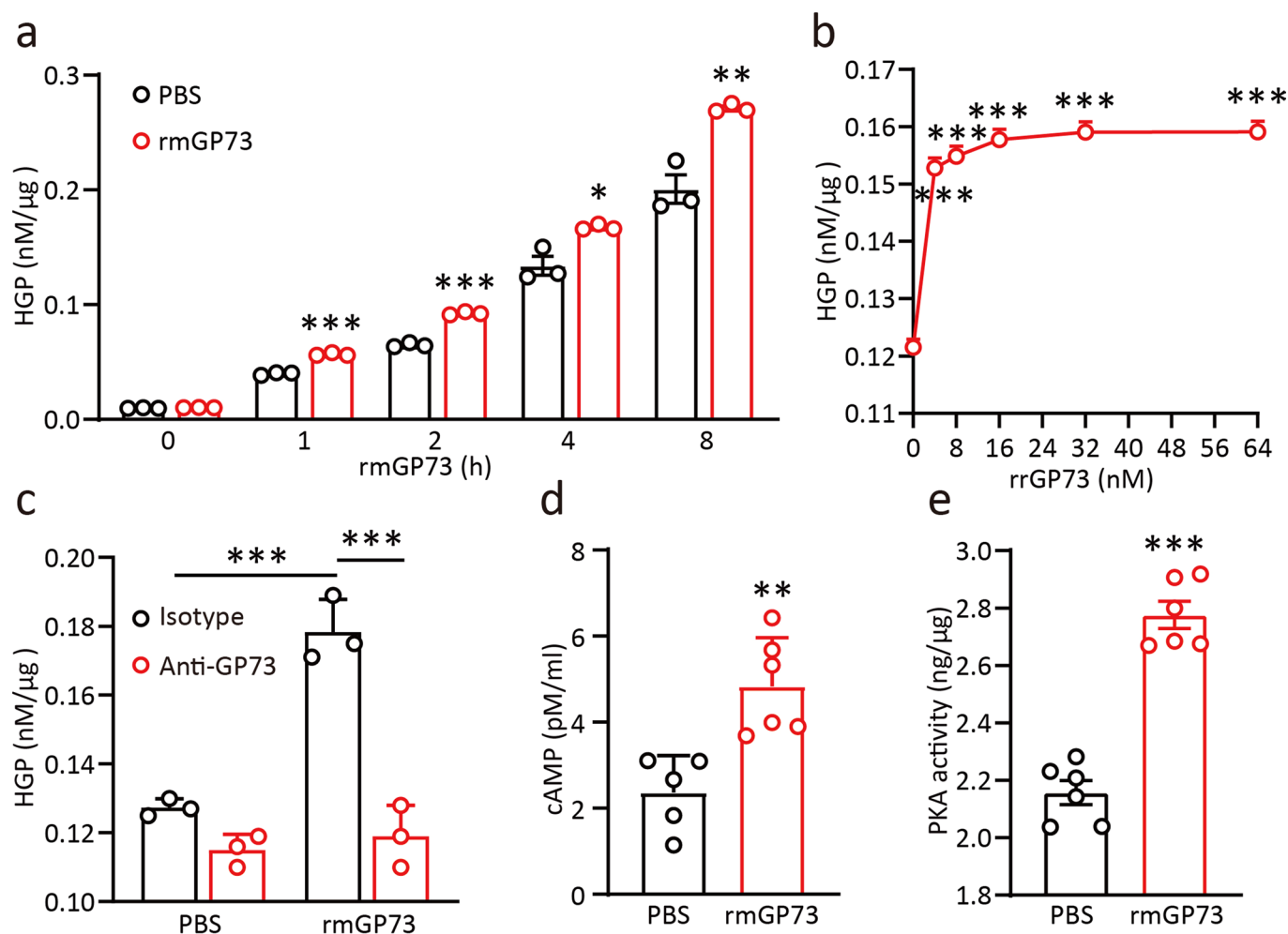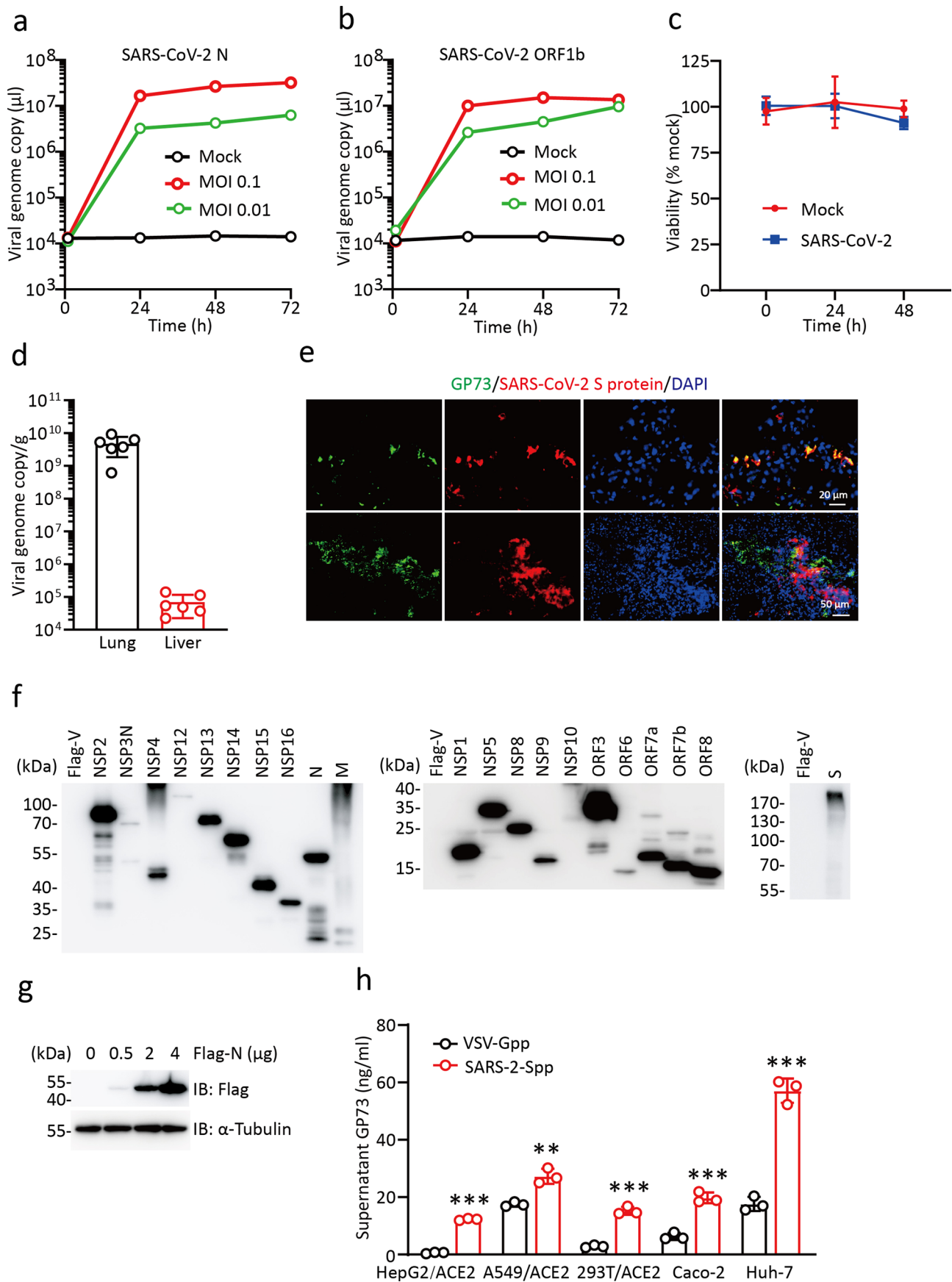
Extended Data Fig. 5 | GP73 stimulates gluconeogenesis. a, Glucose production in PMHs treated with 32 nM rmGP73 for the indicated times. $P = 0.0159$ for rmGP73 versus PBS (4 h), $P = 0.0050$ for rmGP73 versus PBS (8 h), $P < 0.0001$ for rmGP73 versus PBS (1 h and 2 h) by two-tailed Student's t-tests. **b**, Glucose production in primary rat hepatocytes treated with the indicated concentrations of rrGP73 for 2 h. $P < 0.0001$ for 4 nM versus 0 nM, 8 nM versus 0 nM, 16 nM versus 0 nM, 32 nM versus 0 nM and 64 nM versus 0 nM by one-way ANOVA followed by Bonferroni's post hoc test. **c**, Glucose production in PMHs treated with 32 nM rmGP73 with or without anti-GP73 antibody for 2 h. $P = 0.0001$ for rmGP73 versus PBS (isotype), $P < 0.0001$ for anti-GP73 versus isotype (rmGP73) by one-way ANOVA followed by Bonferroni's post hoc test. **d-e**, Intracellular cAMP levels (d) or hepatocyte PKA activity (e) in PMHs treated with 32 nM rmGP73 for 2 h. $P = 0.0031$ for rmGP73 versus PBS (d) and $P < 0.0001$ for rmGP73 versus PBS (e) by two-tailed Student's t-tests. Cell-based studies were performed independently at least three times with comparable results. The data were the means ± SEMs. *$P < 0.05$; **$P < 0.01$; ***$P < 0.001$.
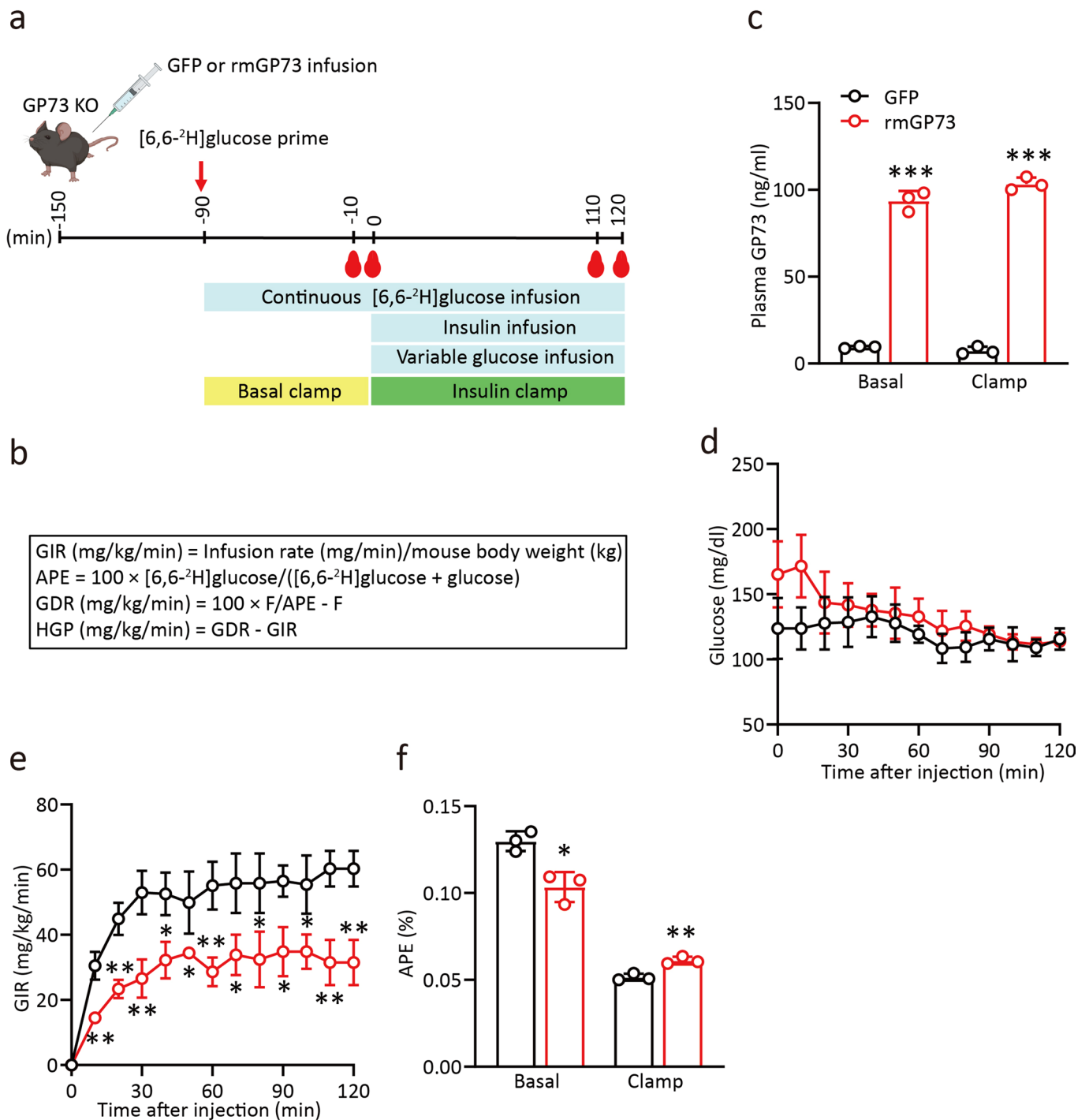
Extended Data Fig. 6 | GP73 stimulates gluconeogenesis. a, Timeline of the procedure for performing the insulin clamp. The figure was created and exported with BioRender.com under a paid subscription. **b**, The equations used to calculate and evaluate insulin sensitivity. **c-f**, GP73 levels (c), blood glucose levels (d), GIR (e), and APE (f) in GP73 KO mice infused with GFP or recombinant GP73 during the clamp study. $P < 0.0001$ for rmGP73 versus GFP (basal and clamp) (c), $P = 0.0029$ for rmGP73 versus GFP (10 min), $P = 0.0028$ for rmGP73 versus GFP (20 min), $P = 0.0068$ for rmGP73 versus GFP (30 min), $P = 0.0150$ for rmGP73 versus GFP (40 min), $P = 0.0489$ for rmGP73 versus GFP (50 min), $P = 0.0059$ for rmGP73 versus GFP (60 min), $P = 0.0258$ for rmGP73 versus GFP (70 min), $P = 0.0315$ for rmGP73 versus GFP (80 min), $P = 0.0137$ for rmGP73 versus GFP (90 min), $P = 0.0264$ for rmGP73 versus GFP (100 min), $P = 0.0049$ for rmGP73 versus GFP (110 min), $P = 0.0049$ for rmGP73 versus GFP (120 min) by two-tailed Student's t-tests (e), $P = 0.0115$ for rmGP73 versus GFP (basal) and $P = 0.0048$ for rmGP73 versus GFP (clamp) (f) by two-tailed Student's t-tests. Hyperinsulinemic-euglycemic clamp studies were performed independently at least three times with comparable results. The data were the means ± SEMs. *$P < 0.05$; **$P < 0.01$; ***$P < 0.001$.

a

b
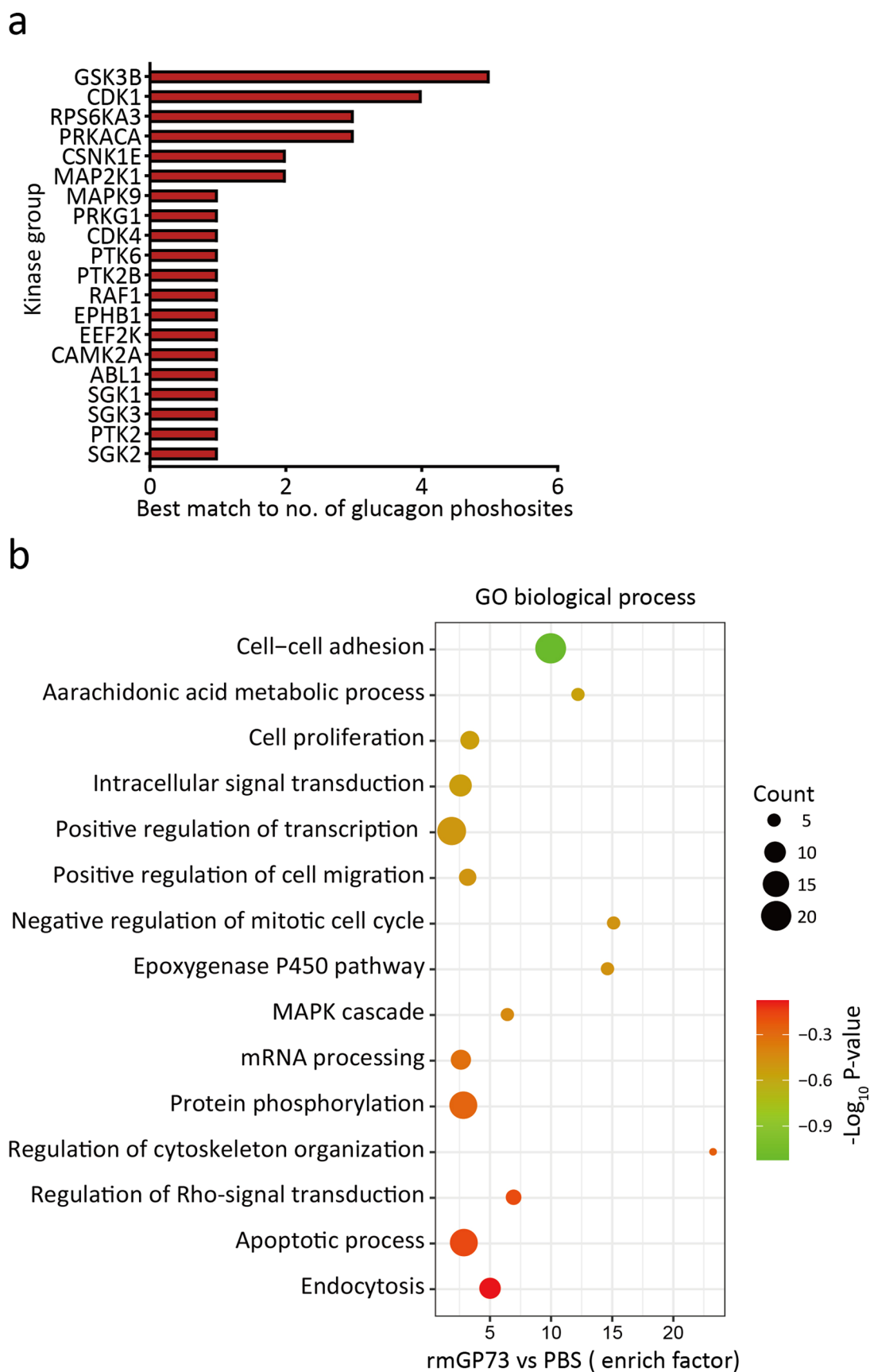
Extended Data Fig. 7 | GP73 induces drastic remodeling of the PKA hub. a, Distribution of matching kinases according to the phosphoproteomics data from the glucagon-treated sample ($P < 0.05$) using Kinase Enrichment Analysis 2 (KEA2) based on one-tailed Fisher's exact test. **b**, GO enriched pathway analysis of significantly regulated phosphopeptides in PMHs treated with rmGP73 ($P < 0.05$) using DAVID Bioinformatics Resources 6.8. The bar plot shows significantly dysregulated pathways.

a GP73 vs PBS Kinases enrichment (KEA2)

b Glucogen vs PBS Kinases enrichment (KEA2)

Extended Data Fig. 8 | GP73 induces drastic remodeling of the PKA hub. a-b, The kinase activity network was constructed according to the phosphoproteomics data from the GP73- (a) or glucagon- (b) treated samples using KEA2.

Extended Data Fig. 9 | See next page for caption.

Extended Data Fig. 9 | SARS-CoV-2 infection promotes GP73 secretion. a-b, SARS-CoV-2 genome copy number per μL using specific primers for N (a) or ORF1b (b) in the supernatants of Huh-7 cells infected with SARS-CoV-2 for the indicated times and MOI. **c**, Cell viability of Huh-7 cells infected with SARS-CoV-2 at 0.1 MOI for the indicated times. **d**, SARS-CoV-2 viral RNAs in liver and lung tissues from mice inoculated with 1.6×10^4 PFU of MASCp6 and sacrificed at day 2 after inoculation (n = 6). **e**, Representative of three images of immunofluorescence staining for GP73 and SARS-CoV-2 S in paraffin-embedded lung tissue from three mice inoculated with 1.6×10^4 PFU of MASCp6 and sacrificed at day 3 after inoculation. **f**, Immunoblotting analysis of GP73 expression in Huh-7 cells transfected with plasmids expressing the indicated SARS-CoV-2 proteins. **g**, Immunoblotting analysis of SARS-CoV-2 N expression in Huh-7 cells transfected with different concentrations of Flag-N. **h**, Supernatant GP73 levels in the indicated human cell lines challenged with SARS-CoV-2pp or VSV-Gpp for 24 h. $P < 0.0001$ for SARS-2-Spp versus VSV-Gpp (HepG2/ACE2), $P = 0.0035$ for SARS-2-Spp versus VSV-Gpp (A549/ACE2), $P = 0.0001$ for SARS-2-Spp versus VSV-Gpp (293 T/ACE2), $P = 0.0005$ for SARS-2-Spp versus VSV-Gpp (Caco-2), $P = 0.0002$ for SARS-2-Spp versus VSV-Gpp (Huh-7) by two-tailed Student's t-tests. Animal and cell-based studies were performed independently at least three times with comparable results. The data were the means ± SEMs. **$P < 0.01$; ***$P < 0.001$.
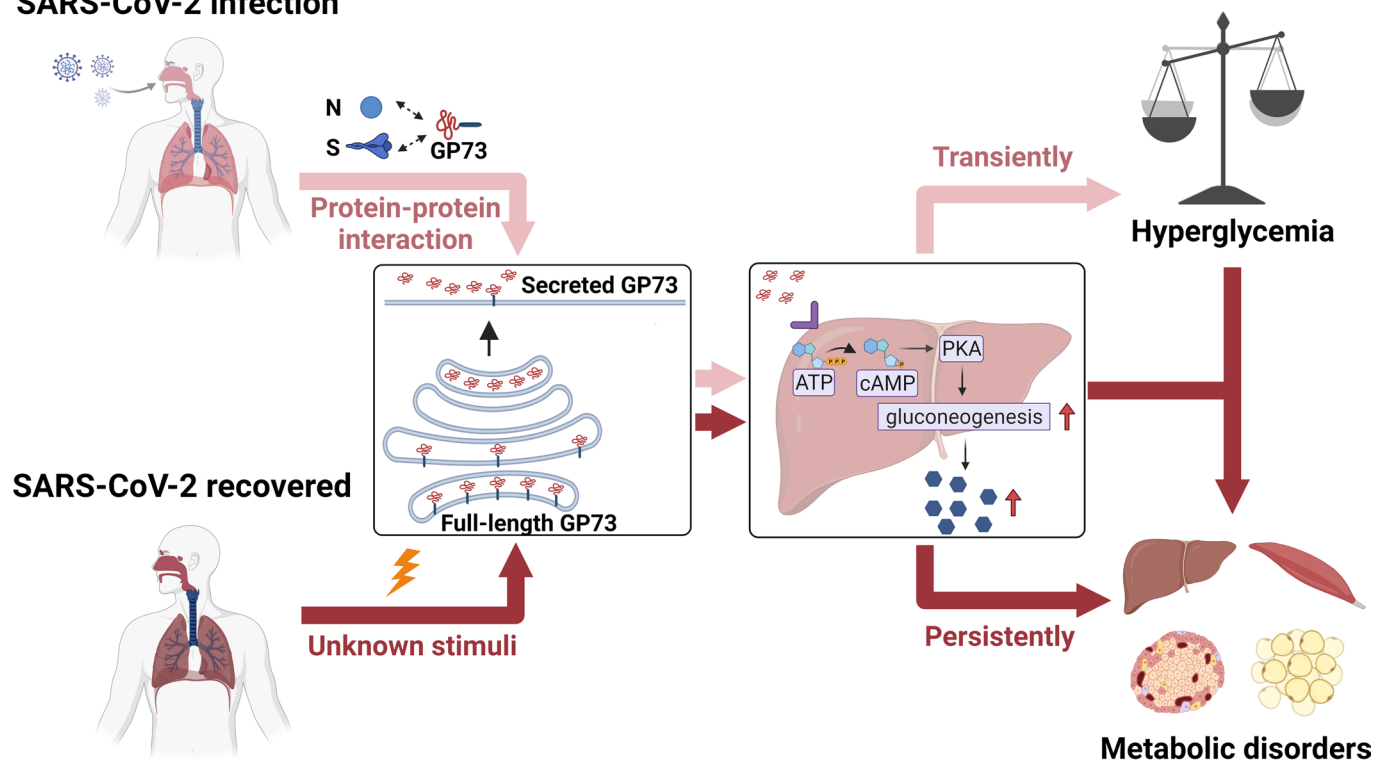
Extended Data Fig. 10 | Hypothetical model of the involvement of GP73 in SARS-CoV-2-induced metabolic disorder. Acute SARS-CoV-2 infection increases the cellular secretion of GP73 via the N and/or S protein. Secreted GP73 traffics to the liver to stimulate gluconeogenesis, leading to hyperglycemia. Sustained GP73 elevation via unknown stimuli may directly predispose the host to metabolic disorders. Targeting GP73 may have therapeutic potential for the treatment of patients with this altered hormone during insulin resistance. The figure was created and exported with BioRender.com under a paid subscription.

Corresponding author(s):   Hui Zhong

Last updated by author(s): Nov 13, 2021

Reporting Summary

Nature Research wishes to improve the reproducibility of the work that we publish. This form provides structure for consistency and transparency in reporting. For further information on Nature Research policies, see our Editorial Policies and the Editorial Policy Checklist.

Statistics

For all statistical analyses, confirm that the following items are present in the figure legend, table legend, main text, or Methods section.

n/a	Confirmed	
☐	☒	The exact sample size (*n*) for each experimental group/condition, given as a discrete number and unit of measurement
☐	☒	A statement on whether measurements were taken from distinct samples or whether the same sample was measured repeatedly
☐	☒	The statistical test(s) used AND whether they are one- or two-sided *Only common tests should be described solely by name; describe more complex techniques in the Methods section.*
☒	☐	A description of all covariates tested
☒	☐	A description of any assumptions or corrections, such as tests of normality and adjustment for multiple comparisons
☐	☒	A full description of the statistical parameters including central tendency (e.g. means) or other basic estimates (e.g. regression coefficient) AND variation (e.g. standard deviation) or associated estimates of uncertainty (e.g. confidence intervals)
☐	☒	For null hypothesis testing, the test statistic (e.g. *F*, *t*, *r*) with confidence intervals, effect sizes, degrees of freedom and *P* value noted *Give P values as exact values whenever suitable.*
☒	☐	For Bayesian analysis, information on the choice of priors and Markov chain Monte Carlo settings
☒	☐	For hierarchical and complex designs, identification of the appropriate level for tests and full reporting of outcomes
☒	☐	Estimates of effect sizes (e.g. Cohen's *d*, Pearson's *r*), indicating how they were calculated

Our web collection on statistics for biologists contains articles on many of the points above.

Software and code

Policy information about availability of computer code

Data collection	Tecan Spark Control (version 2.1), Tanon Gelcap (version 5.22), QuantStudio Design & Analysis Software (version 1.51),Blood glucose reader (ACCU-CHEK, Roche), IVIS® Spectrum In Vivo Imaging System (PerkinElmer), Sciex Triple TOF 6600 (Sciex), Nikon NIS-Elements viewer (version 4.20).
Data analysis	GraphPad Prism (version 8.0), Microsoft Office Standard 2010 (version 14.0.4760.1000), IVIS® Spectrum In Vivo Imaging System Image Software (Version 4.5.5, PerkinElmer), Nikon NIS-Elements AR (version 4.00.12), DAVID Bioinformatics Resources 6.8, Kinase Enrichment Analysis 2 website (KEA2) Cytoscape 3.6.2, STRING (v1.51) , MoMo Modification Motifs 5.3.3, CaseViewer (version 2.4).

For manuscripts utilizing custom algorithms or software that are central to the research but not yet described in published literature, software must be made available to editors and reviewers. We strongly encourage code deposition in a community repository (e.g. GitHub). See the Nature Research guidelines for submitting code & software for further information.

Data

Policy information about availability of data

All manuscripts must include a data availability statement. This statement should provide the following information, where applicable:

- Accession codes, unique identifiers, or web links for publicly available datasets
- A list of figures that have associated raw data
- A description of any restrictions on data availability

The numeric source data are provided in source data files and all of the other data that support the findings of this study are available from the corresponding author upon reasonable request. The phosphoproteomics data have been deposited in iProX database and are accessible through accession number PXD025381.All online datasets used in this study including KEGG (https://www.genome.jp/kegg/), DAVID (https://david.ncifcrf.gov/home.jsp), Cytoscape (https://cytoscape.org/) MoMo (https://meme-suite.org/tools/momo), STRING (https://string-db.org/) and KEA2 (https://www.maayanlab.net/KEA2/).

Field-specific reporting

Please select the one below that is the best fit for your research. If you are not sure, read the appropriate sections before making your selection.

☒ Life sciences   ☐ Behavioural & social sciences   ☐ Ecological, evolutionary & environmental sciences

For a reference copy of the document with all sections, see nature.com/documents/nr-reporting-summary-flat.pdf

Life sciences study design

All studies must disclose on these points even when the disclosure is negative.

Sample size	No sample size calculations were performed. The sample size (n) of each experiment is provided in the corresponding figure captions in the main manuscript and supplementary information files. Sample sizes were chosen to support meaningful conclusions. (PubMed:32494007, 33082294)
Data exclusions	No data were excluded.
Replication	ALL animal experiments were repeated at least two independent times, all attempts at replication were successful. All infection experiments were repeated at least two independent times, all attempts at replication were successful. The western blot and immunoprecipitation assays were repeated at least two independent times, all attempts at replication were successful. The qPCR was performed one time in triplicate all attempts at replication were successful.
Randomization	Allocation into non-treated or treated conditions was random.
Blinding	Technicians were not blinded to group allocation though they were not informed of expected treatment results before and during experimentation. Students blinded their experiments through random numbering of treatment groups and the code was unblinded after analysis.

Behavioural & social sciences study design

All studies must disclose on these points even when the disclosure is negative.

Study description	*Briefly describe the study type including whether data are quantitative, qualitative, or mixed-methods (e.g. qualitative cross-sectional, quantitative experimental, mixed-methods case study).*
Research sample	*State the research sample (e.g. Harvard university undergraduates, villagers in rural India) and provide relevant demographic information (e.g. age, sex) and indicate whether the sample is representative. Provide a rationale for the study sample chosen. For studies involving existing datasets, please describe the dataset and source.*
Sampling strategy	*Describe the sampling procedure (e.g. random, snowball, stratified, convenience). Describe the statistical methods that were used to predetermine sample size OR if no sample-size calculation was performed, describe how sample sizes were chosen and provide a rationale for why these sample sizes are sufficient. For qualitative data, please indicate whether data saturation was considered, and what criteria were used to decide that no further sampling was needed.*
Data collection	*Provide details about the data collection procedure, including the instruments or devices used to record the data (e.g. pen and paper, computer, eye tracker, video or audio equipment) whether anyone was present besides the participant(s) and the researcher, and whether the researcher was blind to experimental condition and/or the study hypothesis during data collection.*
Timing	*Indicate the start and stop dates of data collection. If there is a gap between collection periods, state the dates for each sample cohort.*
Data exclusions	*If no data were excluded from the analyses, state so OR if data were excluded, provide the exact number of exclusions and the rationale behind them, indicating whether exclusion criteria were pre-established.*
Non-participation	*State how many participants dropped out/declined participation and the reason(s) given OR provide response rate OR state that no participants dropped out/declined participation.*
Randomization	*If participants were not allocated into experimental groups, state so OR describe how participants were allocated to groups, and if allocation was not random, describe how covariates were controlled.*

Ecological, evolutionary & environmental sciences study design

All studies must disclose on these points even when the disclosure is negative.

Study description	*Briefly describe the study. For quantitative data include treatment factors and interactions, design structure (e.g. factorial, nested,*

Study description	*hierarchical), nature and number of experimental units and replicates.*
Research sample	*Describe the research sample (e.g. a group of tagged Passer domesticus, all Stenocereus thurberi within Organ Pipe Cactus National Monument), and provide a rationale for the sample choice. When relevant, describe the organism taxa, source, sex, age range and any manipulations. State what population the sample is meant to represent when applicable. For studies involving existing datasets, describe the data and its source.*
Sampling strategy	*Note the sampling procedure. Describe the statistical methods that were used to predetermine sample size OR if no sample-size calculation was performed, describe how sample sizes were chosen and provide a rationale for why these sample sizes are sufficient.*
Data collection	*Describe the data collection procedure, including who recorded the data and how.*
Timing and spatial scale	*Indicate the start and stop dates of data collection, noting the frequency and periodicity of sampling and providing a rationale for these choices. If there is a gap between collection periods, state the dates for each sample cohort. Specify the spatial scale from which the data are taken*
Data exclusions	*If no data were excluded from the analyses, state so OR if data were excluded, describe the exclusions and the rationale behind them, indicating whether exclusion criteria were pre-established.*
Reproducibility	*Describe the measures taken to verify the reproducibility of experimental findings. For each experiment, note whether any attempts to repeat the experiment failed OR state that all attempts to repeat the experiment were successful.*
Randomization	*Describe how samples/organisms/participants were allocated into groups. If allocation was not random, describe how covariates were controlled. If this is not relevant to your study, explain why.*
Blinding	*Describe the extent of blinding used during data acquisition and analysis. If blinding was not possible, describe why OR explain why blinding was not relevant to your study.*

Did the study involve field work? ☐ Yes ☐ No

Field work, collection and transport

Field conditions	*Describe the study conditions for field work, providing relevant parameters (e.g. temperature, rainfall).*
Location	*State the location of the sampling or experiment, providing relevant parameters (e.g. latitude and longitude, elevation, water depth).*
Access & import/export	*Describe the efforts you have made to access habitats and to collect and import/export your samples in a responsible manner and in compliance with local, national and international laws, noting any permits that were obtained (give the name of the issuing authority, the date of issue, and any identifying information).*
Disturbance	*Describe any disturbance caused by the study and how it was minimized.*

Reporting for specific materials, systems and methods

We require information from authors about some types of materials, experimental systems and methods used in many studies. Here, indicate whether each material, system or method listed is relevant to your study. If you are not sure if a list item applies to your research, read the appropriate section before selecting a response.

Materials & experimental systems

n/a	Involved in the study
☐	☒ Antibodies
☐	☒ Eukaryotic cell lines
☒	☐ Palaeontology and archaeology
☐	☒ Animals and other organisms
☐	☒ Human research participants
☒	☐ Clinical data
☒	☐ Dual use research of concern

Methods

n/a	Involved in the study
☒	☐ ChIP-seq
☒	☐ Flow cytometry
☒	☐ MRI-based neuroimaging

Antibodies

Antibodies used	α-Tubulin for immunoblotting (Supplier:SigmaAldrich, Cat: T9026, clone: DM1A, Lot: 078M4796 V) Anti-Flag for immunoblotting (Supplier:SigmaAldrich, Cat: A8592) Anti-glucagon (Supplier:abcam, Cat: ab92517, Lot: GR3208749-11) Anti-insulin (Supplier:abcam, Cat: ab6995) Anti-CREB-phospho S133 (Supplier:abcam, Cat: ab32096, Lot: GR3231215-1) Anti-CREB (Supplier:abcam, Cat:ab32515) Anti-GP73 antibody (Supplier:Santa Cruz F-12, Cat: sc-393372, Lot:) Anti-His antibody (Supplier:Taihua Lekang Biotechnology Cat:KM8001)

Anti-phospho-Akt (Thr308, Supplier:Cell Signaling Technology, Cat:13038, Lot: 11)
Anti-Akt (Supplier:Cell Signaling Technology, Cat:9272, Lot: 5)
Anti-phospho-PKA-C-α (Thr197, Supplier:Cell Signaling Technology, Cat:5661, Lot: 3)
Anti-phospho-PKA substrate (RRXpS/T, Supplier:Cell Signaling Technology, Cat:9624, Lot: 21)
Anti-PKA-C-α (Supplier:Cell Signaling Technology, Cat:5842, Lot:2)
Anti-SARS-CoV / SARS-CoV-2 (COVID-19) spike (Supplier:GeneTex, Cat:GTX632604, clone:1A9, Lot:42219)
Anti-rabbit HRP-IgG (Supplier: ZSGB-BIO, Cat: ZB-2301)
Anti-mouse HRP-IgG (Supplier: ZSGB-BIO, Cat: ZB-2305)
Mouse IgG (Supplier: Beyotime, Cat: A7028)

| Validation | All antibodies are commercially available and were commercially validated. |

α-Tubulin for immunoblotting (Supplier:SigmaAldrich, Cat: T9026, clone: DM1A, Lot: 078M4796 V): Demonstrating antibody specificity through the use of multiple antibodies against target in IHC or ICC. Reacts with bovine, rat, yeast, human, mouse, chicken, fungi and amphibian, suitable for immunofluorescence and western blot.
Anti-Flag for immunoblotting (Supplier:SigmaAldrich, Cat: A8592) : ANTI-FLAG is a registered trademark of Sigma-Aldrich Co. LLC.
Anti-glucagon (Supplier:abcam, Cat: ab92517, Lot: GR3208749-11): Abcam use a variety of methods, including staining multi-normal human tissue microarrays (TMAs), multi-tumor human TMAs, and rat or mouse TMAs during antibody development. These high-throughput arrays allow us to check many tissues at the same time, providing uniformly as all tissues are exposed to the exact same conditions. Also, Abcam are currently working towards using KO cell lines for ICC validation. Reacts with Mouse, Rat and Human.
Anti-insulin (Supplier:abcam, Cat: ab6995): Abcam is leading the way in addressing this with recombinant monoclonal antibodies and knockout edited cell lines for gold-standard validation. The antibody exhibits cross-reactivity with human proinsulin. This antibody recognizes purified insulin from the pancreas of human, bovine, horse, sheep, and proinsulin from human. Cross reaction has been observed with insulin containing cells in fixed sections of pancreas from human, porcine, dog, rabbit, bovine, sheep, rat, guinea pig and cat.
Anti-CREB-phospho S133 (Supplier:abcam, Cat: ab32096, Lot: GR3231215-1): This antibody is specific for CREB phosphorylated on Serine 133. Reacts with: Mouse, Rat, Human. This antibody is a recombinant monoclonal antibody, which offers Improved sensitivity and confirmed specificity. Suitable for: WB, IHC-P, IP, ICC/IF, Flow Cyt (Intra).
Anti-CREB (Supplier:abcam, Cat:ab32515) :This antibody is a recombinant monoclonal antibody, which offers Improved sensitivity and confirmed specificity. KO validated. This antibody recognizes CREB, and can also recognize the splice isoform of CREB. Reacts with: Mouse, Rat, Human. Suitable for: WB, IHC-P.
Anti-GP73 antibody (Supplier:Santa Cruz F-12, Cat: sc-393372, Lot:) : Specific for an epitope mapping between amino acids 330-364 near the C-terminus of GP73 of human origin. Recommended for detection of GP73 of human origin by WB, IP, IF and ELISA.
Anti-His antibody (Supplier:Taihua Lekang Biotechnology Cat:KM8001): The antibody recognizes the His-tag fused to the amino- or carboxy- termini of targeted proteins in transfected or transformed cells. Suitable for: WB, IF.
Anti-phospho-Akt (Thr308, Supplier:Cell Signaling Technology, Cat:13038, Lot: 11): To ensure product performance, CST validate all of our antibodies, in-house, in multiple research applications. Phospho-Akt (Thr308) (D25E6) XP® Rabbit mAb recognizes endogenous levels of Akt1 protein only when phosphorylated at Thr308. Species Reactivity: Human, Mouse, Rat, Monkey. Suitable for: WB, IP, IF, Flow Cyt.
Anti-Akt (Supplier:Cell Signaling Technology, Cat:9272, Lot: 5): To ensure product performance, CST validate all of our antibodies, in-house, in multiple research applications. Akt Antibody detects endogenous levels of total Akt1, Akt2 and Akt3 proteins. The antibody does not cross-react with related kinases. Species Reactivity: Human, Mouse, Rat, Hamster, Monkey, Chicken, D. melanogaster, Bovine, Dog, Pig, Guinea Pig. Suitable for: WB, IP, IF, Flow Cyt.
Anti-phospho-PKA-C-α (Thr197, Supplier:Cell Signaling Technology, Cat:5661, Lot: 3): To ensure product performance, CST validate all of our antibodies, in-house, in multiple research applications. Phospho-PKA C (Thr197) (D45D3) Rabbit mAb detects endogenous levels of PKA C (-α, -β, and -γ) only when phosphorylated at Thr197. Species Reactivity: Human, Mouse, Rat, Monkey. Suitable for: WB.
Anti-phospho-PKA substrate (RRXpS/T, Supplier:Cell Signaling Technology, Cat:9624, Lot: 21): To ensure product performance, CST validate all of our antibodies, in-house, in multiple research applications. Phospho-PKA Substrate (RRXS*/T*) (100G7E) Rabbit mAb detects peptides and proteins containing a phospho-Ser/Thr residue with arginine at the -3 and -2 positions. It is a useful tool in identifying new substrates of PKA. The antibody recognizes other -3 arginine-bearing phospho-Ser/Thr peptides, such as substrate motifs for Akt and PKC, to a lesser extent. It does not recognize the nonphosphorylated substrate motif peptides. (U.S. Patent No's.: 6,441,140; 6,982,318; 7,259,022; 7,344,714; U.S.S.N. 11,484,485; and all foreign equivalents.) Species Reactivity: All Species Expected. Suitable for: WB, IP.
Anti-PKA-C-α (Supplier:Cell Signaling Technology, Cat:5842, Lot:2) : To ensure product performance, CST validate all of our antibodies, in-house, in multiple research applications. PKA C-α (D38C6) Rabbit mAb recognizes endogenous levels of total PKA C-α protein. Species Reactivity: Human, Mouse, Rat, Hamster, Monkey. Suitable for: WB, IP.
Anti-SARS-CoV / SARS-CoV-2 (COVID-19) spike (Supplier:GeneTex, Cat:GTX632604, clone:1A9, Lot:42219) : Overexpression validation. This antibody detects both SARS-CoV spike and SARS-CoV-2 spike proteins (S2 subunit). Our internal testing indicates no cross-reactivity with MERS-CoV spike protein.   Suitable for: WB, ICC/IF, IHC-P, FACS, IP, ELISA, EM, Sandwich ELISA, IHC-P.
Anti-rabbit HRP-IgG (Supplier: ZSGB-BIO, Cat: ZB-2301)
Anti-mouse HRP-IgG (Supplier: ZSGB-BIO, Cat: ZB-2305)
Mouse IgG (Supplier: Beyotime, Cat: A7028)

Eukaryotic cell lines

Policy information about cell lines

| Cell line source(s) | The HepG2 (CRL-10741), Vero E6 (CRL-1586), Caco-2 (HTB-37), A549 (CCL-185), 293T (CRL-3216) and L6 (CRL-1658) cell lines were obtained from the American Type Culture Collection (ATCC, Rockville, MD, USA). The Huh-7 (0403) cell line was obtained from the Japanese Collection of Research Bioresources. |
| Authentication | HepG2, Caco-2, A549, 293T and Huh-7 cell lines were authenticated by STR profiling. |

Mycoplasma contamination	All cell lines have no mycoplasma contamination .
Commonly misidentified lines (See ICLAC register)	No commonly misidentified lines were used.

Palaeontology and Archaeology

Specimen provenance	*Provide provenance information for specimens and describe permits that were obtained for the work (including the name of the issuing authority, the date of issue, and any identifying information).*
Specimen deposition	*Indicate where the specimens have been deposited to permit free access by other researchers.*
Dating methods	*If new dates are provided, describe how they were obtained (e.g. collection, storage, sample pretreatment and measurement), where they were obtained (i.e. lab name), the calibration program and the protocol for quality assurance OR state that no new dates are provided.*

☐ Tick this box to confirm that the raw and calibrated dates are available in the paper or in Supplementary Information.

Ethics oversight	*Identify the organization(s) that approved or provided guidance on the study protocol, OR state that no ethical approval or guidance was required and explain why not.*

Note that full information on the approval of the study protocol must also be provided in the manuscript.

Animals and other organisms

Policy information about studies involving animals; ARRIVE guidelines recommended for reporting animal research

Laboratory animals	Male C57BL/6N WT mice (8 to 10 weeks old) and BALB/c mice (9 months old) were purchased from SPF Biotechnology (Beijing, China). Male GP73 KO mice (T20200316-18[D25], 8 to 10 weeks old) were generated from C57BL/6N WT mice human by Southern Model Biotechnology (Shanghai, China). All mice were group-housed conventionally on a 12-h light/dark cycle for 3 days before any experiments, the environmental conditions were maintained thermostatically between 18?-23? with 40%-60% humidity.
Wild animals	NO
Field-collected samples	NO
Ethics oversight	All C57BL/6N animal experiments were performed at the AMMS Animal Center (Beijing, China) and were approved by the Institutional Animal Care and Use Committee. BALB/c infected by mouse-adapted SARS-CoV-2 strain MASCp6 were conducted in the Biosafety Level 3 laboratory (BSL-3) and approved by the Animal Experiment Committee of Laboratory Animal Center, Beijing Institute of Microbiology and Epidemiology (approval number: IACUC-DWZX2020-002).

Note that full information on the approval of the study protocol must also be provided in the manuscript.

Human research participants

Policy information about studies involving human research participants

Population characteristics	Basic information, serum biochemical test results and blood samples for GP73 and glucose level analysis were collected from 76 COVID-19 patients at Huoshenshan Hospital (Wuhan, Hubei province, People's Republic of China) from January 11 to March 11, 2020 at admission before any intervention. Diagnosis was based on chest computed tomography (CT) manifestations and/or reverse transcription-polymerase chain reaction (RT-PCR) according to the criteria of the New Coronavirus Pneumonia Prevention and Control Program (5th edition) published by the National Health Commission of China. According to these criteria, COVID-19 patients were classified into mild, moderate and severe COVID-19 subgroups. The majority of patients received combined treatments, including antiviral drugs (lopinavir/ritonavir, interferon-α, arbidol), herbs, intravenous immunoglobulin and antibiotics. Data were excluded if the subject was younger than 18 years or older than 75 years, had incomplete medical records, acute lethal organ injury (e.g., acute myocardial infarction, acute coronary syndrome, acute pulmonary embolism, or acute stroke), or decompensated or end-stage chronic organ dysfunction (e.g., decompensated cirrhosis, decompensated chronic renal insufficiency, or severe congestive heart failure), was pregnant, was HBV-, HCV- or HIV-positive, used drugs with known effects on glucose metabolism (glucocorticoid or tocilizumab) or had malignancy (Supplementary Table 1). Twenty-eight patients had mild COVID-19, 36 patients had moderate COVID-19, and 12 patients had severe COVID-19 (Supplementary Table 2). Among them, 4 patients with moderate COVID-19 and 9 patients with severe COVID-19 were enrolled, and blood samples were collected at admission before any intervention, during hospitalization and after recovery before discharge. The discharge criteria included normal temperature, resolved respiratory symptoms, improved CT images, and two consecutively negative RT-PCR results for SARS-CoV-2 in respiratory tract specimens within an interval of at least 24 h.
Recruitment	76 COVID-19 patients at Huoshenshan Hospital (Wuhan, Hubei province, People's Republic of China) from January 11 to March 11, 2020 at admission before any intervention. Diagnosis was based on chest computed tomography (CT) manifestations and/or reverse transcription-polymerase chain reaction (RT-PCR) according to the criteria of the New Coronavirus Pneumonia Prevention and Control Program (5th edition) published by the National Health Commission of China. According to these criteria, COVID-19 patients were classified into mild, moderate and severe COVID-19 subgroups.
Ethics oversight	The Ethics Committee of Huoshenshan Hospital approved the study (HSSLL036). Given the urgency of the COVID-19

| Ethics oversight | pandemic, the need for informed consent forms was waived by the ethics boards of the hospitals. |

Note that full information on the approval of the study protocol must also be provided in the manuscript.

Clinical data

Policy information about clinical studies

All manuscripts should comply with the ICMJE guidelines for publication of clinical research and a completed CONSORT checklist must be included with all submissions.

Clinical trial registration	*Provide the trial registration number from ClinicalTrials.gov or an equivalent agency.*
Study protocol	*Note where the full trial protocol can be accessed OR if not available, explain why.*
Data collection	*Describe the settings and locales of data collection, noting the time periods of recruitment and data collection.*
Outcomes	*Describe how you pre-defined primary and secondary outcome measures and how you assessed these measures.*

Dual use research of concern

Policy information about dual use research of concern

Hazards

Could the accidental, deliberate or reckless misuse of agents or technologies generated in the work, or the application of information presented in the manuscript, pose a threat to:

No | Yes
- [ ] | [ ] Public health
- [ ] | [ ] National security
- [ ] | [ ] Crops and/or livestock
- [ ] | [ ] Ecosystems
- [ ] | [ ] Any other significant area

Experiments of concern

Does the work involve any of these experiments of concern:

No | Yes
- [ ] | [ ] Demonstrate how to render a vaccine ineffective
- [ ] | [ ] Confer resistance to therapeutically useful antibiotics or antiviral agents
- [ ] | [ ] Enhance the virulence of a pathogen or render a nonpathogen virulent
- [ ] | [ ] Increase transmissibility of a pathogen
- [ ] | [ ] Alter the host range of a pathogen
- [ ] | [ ] Enable evasion of diagnostic/detection modalities
- [ ] | [ ] Enable the weaponization of a biological agent or toxin
- [ ] | [ ] Any other potentially harmful combination of experiments and agents

ChIP-seq

Data deposition

- [ ] Confirm that both raw and final processed data have been deposited in a public database such as GEO.

- [ ] Confirm that you have deposited or provided access to graph files (e.g. BED files) for the called peaks.

Data access links *May remain private before publication.*	*For "Initial submission" or "Revised version" documents, provide reviewer access links. For your "Final submission" document, provide a link to the deposited data.*
Files in database submission	*Provide a list of all files available in the database submission.*
Genome browser session (e.g. UCSC)	*Provide a link to an anonymized genome browser session for "Initial submission" and "Revised version" documents only, to enable peer review. Write "no longer applicable" for "Final submission" documents.*

Methodology

| Replicates | *Describe the experimental replicates, specifying number, type and replicate agreement.* |

Sequencing depth	*Describe the sequencing depth for each experiment, providing the total number of reads, uniquely mapped reads, length of reads and whether they were paired- or single-end.*
Antibodies	*Describe the antibodies used for the ChIP-seq experiments; as applicable, provide supplier name, catalog number, clone name, and lot number.*
Peak calling parameters	*Specify the command line program and parameters used for read mapping and peak calling, including the ChIP, control and index files used.*
Data quality	*Describe the methods used to ensure data quality in full detail, including how many peaks are at FDR 5% and above 5-fold enrichment.*
Software	*Describe the software used to collect and analyze the ChIP-seq data. For custom code that has been deposited into a community repository, provide accession details.*

Flow Cytometry

Plots

Confirm that:

☒ The axis labels state the marker and fluorochrome used (e.g. CD4-FITC).

☒ The axis scales are clearly visible. Include numbers along axes only for bottom left plot of group (a 'group' is an analysis of identical markers).

☒ All plots are contour plots with outliers or pseudocolor plots.

☒ A numerical value for number of cells or percentage (with statistics) is provided.

Methodology

Sample preparation	*Describe the sample preparation, detailing the biological source of the cells and any tissue processing steps used.*
Instrument	*Identify the instrument used for data collection, specifying make and model number.*
Software	*Describe the software used to collect and analyze the flow cytometry data. For custom code that has been deposited into a community repository, provide accession details.*
Cell population abundance	*Describe the abundance of the relevant cell populations within post-sort fractions, providing details on the purity of the samples and how it was determined.*
Gating strategy	*Describe the gating strategy used for all relevant experiments, specifying the preliminary FSC/SSC gates of the starting cell population, indicating where boundaries between "positive" and "negative" staining cell populations are defined.*

☒ Tick this box to confirm that a figure exemplifying the gating strategy is provided in the Supplementary Information.

Magnetic resonance imaging

Experimental design

Design type	*Indicate task or resting state; event-related or block design.*
Design specifications	*Specify the number of blocks, trials or experimental units per session and/or subject, and specify the length of each trial or block (if trials are blocked) and interval between trials.*
Behavioral performance measures	*State number and/or type of variables recorded (e.g. correct button press, response time) and what statistics were used to establish that the subjects were performing the task as expected (e.g. mean, range, and/or standard deviation across subjects).*

Acquisition

Imaging type(s)	*Specify: functional, structural, diffusion, perfusion.*
Field strength	*Specify in Tesla*
Sequence & imaging parameters	*Specify the pulse sequence type (gradient echo, spin echo, etc.), imaging type (EPI, spiral, etc.), field of view, matrix size, slice thickness, orientation and TE/TR/flip angle.*
Area of acquisition	*State whether a whole brain scan was used OR define the area of acquisition, describing how the region was determined.*

Diffusion MRI   ☐ Used   ☐ Not used

Preprocessing

Preprocessing software
Provide detail on software version and revision number and on specific parameters (model/functions, brain extraction, segmentation, smoothing kernel size, etc.).

Normalization
If data were normalized/standardized, describe the approach(es): specify linear or non-linear and define image types used for transformation OR indicate that data were not normalized and explain rationale for lack of normalization.

Normalization template
Describe the template used for normalization/transformation, specifying subject space or group standardized space (e.g. original Talairach, MNI305, ICBM152) OR indicate that the data were not normalized.

Noise and artifact removal
Describe your procedure(s) for artifact and structured noise removal, specifying motion parameters, tissue signals and physiological signals (heart rate, respiration).

Volume censoring
Define your software and/or method and criteria for volume censoring, and state the extent of such censoring.

Statistical modeling & inference

Model type and settings
Specify type (mass univariate, multivariate, RSA, predictive, etc.) and describe essential details of the model at the first and second levels (e.g. fixed, random or mixed effects; drift or auto-correlation).

Effect(s) tested
Define precise effect in terms of the task or stimulus conditions instead of psychological concepts and indicate whether ANOVA or factorial designs were used.

Specify type of analysis: ☐ Whole brain ☐ ROI-based ☐ Both

Statistic type for inference
(See Eklund et al. 2016)
Specify voxel-wise or cluster-wise and report all relevant parameters for cluster-wise methods.

Correction
Describe the type of correction and how it is obtained for multiple comparisons (e.g. FWE, FDR, permutation or Monte Carlo).

Models & analysis

n/a	Involved in the study
☐	☐ Functional and/or effective connectivity
☐	☐ Graph analysis
☐	☐ Multivariate modeling or predictive analysis

Functional and/or effective connectivity
Report the measures of dependence used and the model details (e.g. Pearson correlation, partial correlation, mutual information).

Graph analysis
Report the dependent variable and connectivity measure, specifying weighted graph or binarized graph, subject- or group-level, and the global and/or node summaries used (e.g. clustering coefficient, efficiency, etc.).

Multivariate modeling and predictive analysis
Specify independent variables, features extraction and dimension reduction, model, training and evaluation metrics.